

Review article

Wilhelm Pfleging*

A review of laser electrode processing for development and manufacturing of lithium-ion batteries

<https://doi.org/10.1515/nanoph-2017-0044>

Received April 21, 2017; revised September 11, 2017; accepted October 8, 2017

Abstract: Laser processes for cutting, annealing, structuring, and printing of battery materials have a great potential in order to minimize the fabrication costs and to increase the electrochemical performance and operational lifetime of lithium-ion cells. Hereby, a broad range of applications can be covered such as micro-batteries, mobile applications, electric vehicles, and stand-alone electric energy storage devices. Cost-efficient nanosecond (ns)-laser cutting of electrodes was one of the first laser technologies which were successfully transferred to industrial high-energy battery production. A defined thermal impact can be useful in electrode manufacturing which was demonstrated by laser annealing of thin-film electrodes for adjusting of battery active crystalline phases or by laser-based drying of composite thick-film electrodes for high-energy batteries. Ultrafast or ns-laser direct structuring or printing of electrode materials is a rather new technical approach in order to realize three-dimensional (3D) electrode architectures. Three-dimensional electrode configurations lead to a better electrochemical performance in comparison to conventional 2D one, due to an increased active surface area, reduced mechanical tensions during electrochemical cycling, and an overall reduced cell impedance. Furthermore, it was shown that for thick-film composite electrodes an increase of electrolyte wetting could be achieved by introducing 3D micro-/nano-structures. Laser structuring can turn electrodes into superwicking. This has a positive impact regarding an increased battery lifetime and a reliable battery production. Finally, laser processes can be up-scaled in order to transfer the

3D battery concept to high-energy and high-power lithium-ion cells.

Keywords: laser processing; thin films; composite thick films; electrode; lithium-ion battery.

1 Introduction

Twenty-seven years ago, Sony introduced for portable electronic applications a high-voltage (3.7 V) and high-energy (HE) lithium-ion battery (LIB) based on graphite anode (Li_xC_6), lithium cobalt oxide ($\text{Li}_{1-x}\text{CoO}_2$) as cathode, and non-aqueous liquid electrolyte. Since then, LIBs rose as an essential tool for the storage of electric energy [1–3]. Currently, LIBs drag attention as green energy sources in pollution-free electrical vehicles. Electromobility appears today as a viable solution in the frame of new mobility concepts for sustainable use of energy resources and environmental protection, and LIB technology seems to be the energy storage concept with the potential to meet the future requirements of the automotive industry in terms of energy and power density [4]. In modern lithium-ion cells, thick-film electrodes (cathode, anode) are complex multi-material systems with defined material components, grain sizes, porosities, and pore size distributions in the micrometer and submicrometer range. State-of-the-art batteries with pouch cell design or prismatic cells for high-power applications consist of thick-film electrode stacks with capacities up to 60 Ah or even higher [5].

In cell manufacturing there are numerous production steps, which could be covered or supported by laser technologies (Figure 1): contour cutting, notching, slotting, structuring, welding, and marking [6]. The main advantages of laser materials processing are rapid manufacturing, high process reliability, and design flexibility. To become accepted in commercial battery manufacturing, the laser processes should improve or at least maintain the battery performance and safety. Finally, an economic laser-based process technology should be realized in order to achieve a reduction of the overall LIB

*Corresponding author: Wilhelm Pfleging, Karlsruhe Institute of Technology, IAM-AWP, P.O. Box 3640, 76021 Karlsruhe, Germany; and Karlsruhe Nano Micro Facility, H.-von-Helmholtz-Platz 1, 76344 Egg.-Leopoldshafen, Germany, e-mail: wilhelm.pfleging@kit.edu. <http://orcid.org/0000-0002-9221-9493>

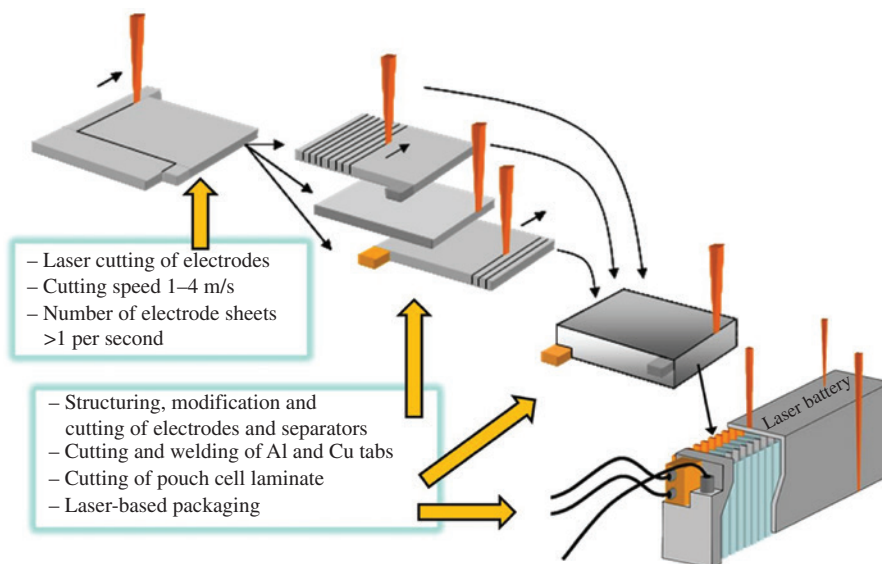


Figure 1: Laser-supported production steps for manufacturing of lithium-ion cells in pouch cell design.

manufacturing costs. These requirements can be reached by the recently developed laser cutting, notching, and slotting of electrodes for commercial battery manufacturing. Nevertheless, laser technologies always compete with conventional technologies (such as mechanical blanking) regarding the size of investment, period of amortization, the functional aspects, operating lifetime, and related cell performance, which will finally decide a successful integration in battery production lines.

Laser welding processes such as tap welding, welding of battery housing, and welding of up to 100 current collector flags are intensively investigated and already introduced in some battery manufacturing lines [7–9]. Even so, state-of-the-art tap welding or welding of current collector stacks is still represented by ultrasonic welding [6]. For future HE cells using thick-film composite electrodes the laser-assisted welding will become more interesting due to the fact that the ultrasonic device may induce ultrasonic induced damages, cracks, or film delamination, to thick and brittle composite electrodes. Non-contacting laser welding methods with local thermal impact may overcome these drawbacks.

Laser welding and laser cutting in cell manufacturing are intended not to have a significant impact on the cell performance. The main intention of these processes is to make the production more reliable and to reduce production cost. This is in contrast to the new idea of laser modification of battery materials, which are directly involved in cell operation. Modification of active material, current collectors, and separators will influence the performance and cell functionality. This is a rather new scientific and

technical approach: laser structuring of current collectors (aluminum or copper), coated separator materials, and thin- or thick-film electrodes such as $\text{LiNi}_{1/3}\text{Mn}_{1/3}\text{Co}_{1/3}\text{O}_2$ (NMC-111), LiFePO_4 (LFP), LiCoO_2 (LCO), LiMn_2O_4 (LMO), and silicon [10–14]. It could be shown for thin-film and thick-film batteries that laser-generated micro- and nanostructures can improve battery lifetime, cycle stability, and high rate capability. The structuring of current collectors made of aluminum or copper can be used to improve the electrode film adhesion which is a critical aspect for HE and thick-film electrodes [15]. Direct structuring of electrode films represents a new battery design concept which can be described as three-dimensional (3D) concept (“3D battery”) for increasing areal energy capacities and power densities [16–19]. Three-dimensional architectures in LIBs can, for example, increase lithium-ion diffusion, reduce cell impedance [16], and compensate mechanical tensions due to volume changes resulting from lithium-ion insertion and de-insertion during cell operation [20]. The 3D battery concept is extended by introducing capillary structures or artificial porosity in active material in order to achieve an enhancement of electrolyte wetting properties [21]. Both the improvement in lithium-ion diffusion kinetics and the turn of battery materials into superwicking deliver advanced battery performances which will be a central aspect for advanced battery production. Electrochemical analysis showed that a steep rise of capacity retention at high charging and discharging currents and an increased cell lifetime can be obtained in comparison to standard cells with unstructured battery materials. In this review article, recent developments based on laser

processing of battery materials will be presented, and their impact on battery performance will be discussed.

2 Short overview of lithium-battery technology and materials

The performance of LIBs is mainly defined by the so-called active materials. In commercial battery manufacturing, the active materials and other constituents are composed according to special and generally inaccessible recipes. Hereby, licensing rights and patent application play an important role. In general, secondary lithium-ion cells utilize cathode materials such as lithium manganese oxide LiMn_2O_4 (LMO), lithium nickel oxide LiNiO_2 , lithium nickel manganese cobalt oxide $\text{LiNi}_{1/3}\text{Mn}_{1/3}\text{Co}_{1/3}\text{O}_2$ (NMC), lithium iron phosphate LiFePO_4 (LFP), or lithium cobalt oxide LiCoO_2 (LCO) [22]. Differences can be found in the type of lithium-ion diffusion paths. The olivine-type LFP and some silicon derivatives provide one-dimensional diffusion paths, whereas the layered compounds (NMC, LCO) two-dimensional and the spinel-type (LMO) 3D paths [23]. The practical capacities also differ as a function of active materials, counting 160 mAh/g for NMC, 120 mAh/g for

LMO, 145 mAh/g for LCO, and 165 mAh/g for LFP [24]. In state-of-the-art LIBs, graphite is used as counter electrode, with a practical capacity of about 330 mAh/g.

In order to describe the functionality of a lithium-ion cell, one has to distinguish between charging and discharging. During charging, lithium-ions diffuse from the cathode, e.g. LiCoO_2 , to the graphite electrode (the anode) forming lithiated graphite (Li_xC_6). This in turn means that during charging the cathode material gets delithiated, forming $\text{Li}_{1-x}\text{CoO}_2$ (Figure 2). The maximum uptake of Li by graphite is one lithium per graphene unit (LiC_6), which corresponds to the maximum state of charge (SoC). During discharging the reverse process takes place, and one receives the LiCoO_2 cathode structure at the end of the discharge process (0% SoC). There is the convention that the electrodes are designated at the discharge, i.e. the negative electrode as the anode and the positive electrode as the cathode. The anode undergoes oxidation, while the cathode sees a reduction. During charge and discharge, lithium-ions shuttle reversibly between two host structures, and therefore batteries with LiCoO_2 cathodes and graphite anodes are also called “rocking-chair system” with a working potential of about 4 V.

The gravimetric or specific energy density, in Wh/kg, is one of the important key parameters of batteries. It

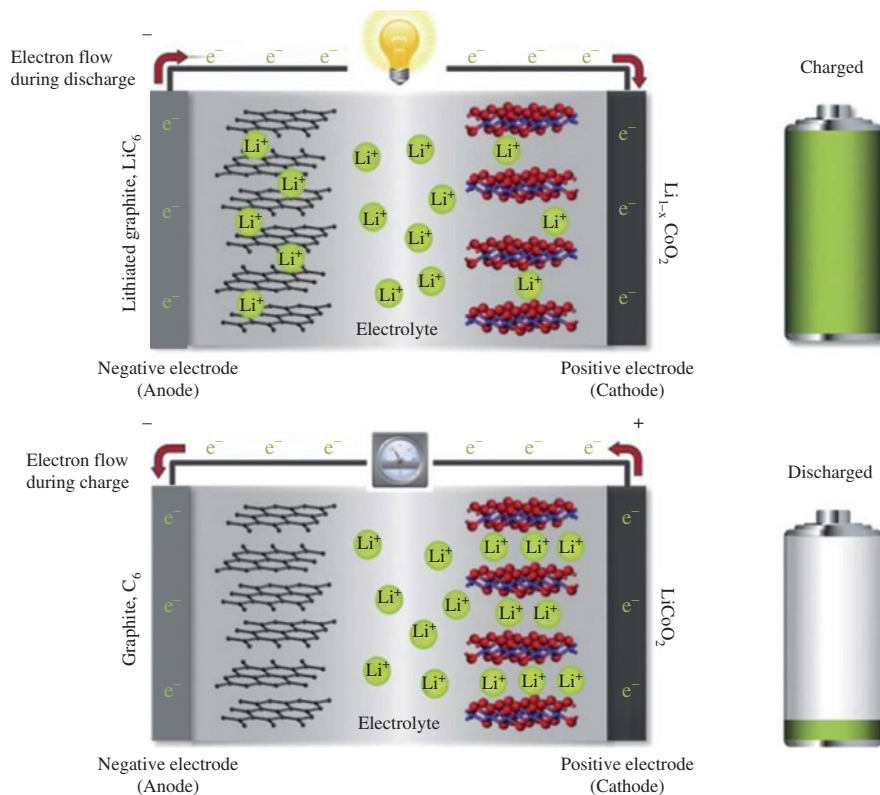


Figure 2: Schematic view of the principle of operation of a lithium-ion cell. Reprinted from [25].

defines the amount of lithium-ions, which can be transferred within the charged battery at a certain voltage. For NMC the theoretical value for specific capacity Q/m can be calculated using the Faraday constant F and the molar mass M of the active material:

$$\frac{Q}{m} = \frac{F}{M} \quad (1)$$

with molar mass M for NMC, $M = 96.461$ g/mol and Faraday constant, $F = 96,485$ As/mol, the theoretical value for NMC becomes $Q/m = 278$ mAh/g.

Due to the fact that in the battery operating voltage window (3–4.2 V) only 58% of the lithium-ions can be extracted, the practical specific capacity drops down to $Q_{\text{exp}}/m = 160$ mAh/g [24]. This value is still referred to the active mass of NMC and does not take into account inactive materials such as current collectors, electrolyte, counter electrode, and battery housing. Related to an average operating voltage for NMC of $U = 3.7$ V [24], one receives a practical gravimetric energy density on material level of about $U \cdot Q_{\text{exp}}/m = 592$ Wh/kg.

This value has to be corrected still, taking into account the inactive cell components. Referring to technical data listed by Wood et al. [26], one can calculate the weight of the individual cell components for a HE 52 Ah cell (Table 1).

On electrode level, including weight of binder, additives, and aluminum current collector, the weight of NMC counts 64% of the weight of the entire electrode. Furthermore, the weight of the active material NMC is almost a third of the weight of the whole cell. This becomes even more worse on battery level including housing, electrical connections, and battery management system. The specific energy density of the present battery packs is nearly four times smaller than the energy density on material level [4]. Figure 3 reveals these different levels and the big gap (factor 4) between theoretical and practical energy density of state-of-the-art LIBs.

Table 1: Weight of components in a 52 Ah pouch cell, total weight 1140 g. Data extracted from [26].

NMC	347 g
Graphite	171 g
Copper	154 g
Aluminum	110 g
Separator	52 g
Binder and additives	57 g
Electrolyte	249 g

Laminate material for pouch assembly is not taken into account.

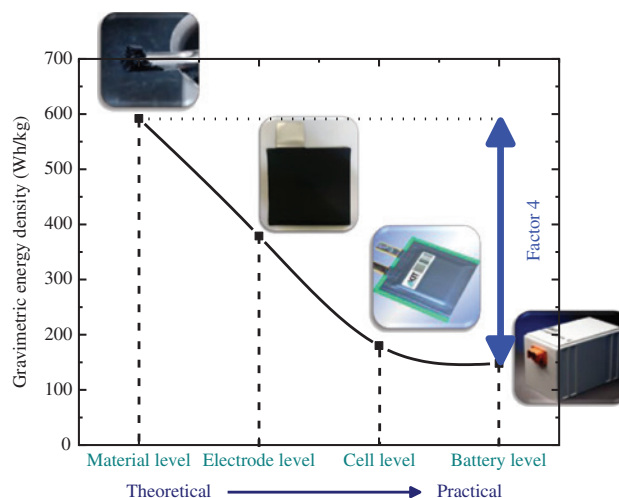


Figure 3: Theoretical [see equation (1)] and practical gravimetric energy density of NMC based on a standard 52 Ah pouch cell [26] and state-of-the-art battery packs [4].

In recent research, the main target for applications in electrical vehicles is to develop cells with energy densities of about 250–350 Wh/kg on cell level [27]. Besides the development of new types of HE cathode materials, e.g. HE NMC, and HE anode materials, e.g. Si-doped graphite, an engineering challenge is also taken into account: a significant reduction of factor 4 in Figure 3 should be possible by developing new cell architectures, by increasing the electrode thickness, and by reducing the amount of inactive material. The combination of material development and engineering tasks will be the most promising approach for next generation batteries.

3 Thin-film and thick-film electrodes

The concept of a “thin-film electrode” is in general connected to the term “micro-battery” (Figure 4). Micro-batteries are used for small-scale and low-energy applications, e.g. micro- and nano-electromechanical systems [19, 28]. The thickness of the individual compact electrodes is limited to a few micrometers (Figure 4) due to the fact that higher thicknesses would lead to crack formation and film failure caused by mechanical stress.

According to a review article of Patil et al. [29], the first rechargeable all-solid state thin-film batteries have been developed in 1983 by Kanehori et al. from Hitachi Co. [30]. They consisted of a TiS_2 cathode prepared by chemical vapor deposition (CVD), an amorphous $\text{Li}_{3.6}\text{Si}_{0.6}\text{P}_{0.4}\text{O}_4$

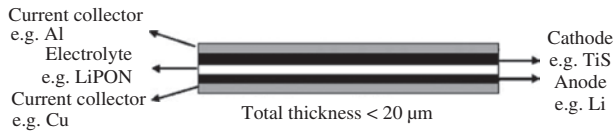


Figure 4: Schematic diagram of a stacked thin-film lithium-ion cell. Reprinted from [28].

glass electrolyte by radio frequency (rf) magnetron sputtering and lithium metal as anode deposited by vacuum evaporation (Figure 4). Pulsed laser deposition (PLD) is conceptually a simple deposition tool for thin films and multilayers. With the use of PLD, artificially layered materials and metastable phases have been created, and the control of film composition and new material combinations were enabled [31, 32]. The potential of thin PLD films for electrochemical applications has been recognized [33–35], and the number of studies is increasing steadily. The reason for the late recognition of PLD films for electrochemical studies is probably related to the fact that many electrochemical studies are associated with wet chemistry, i.e. liquid electrolytes, while PLD is a vacuum technique, and very often ultra-high vacuum analytical methods are applied for the PLD films. The first application of PLD as a deposition technique for LIB-related materials, studying mainly materials used as cathodes, was published at the end of the 1990s [36]. Only in the last few years, materials for anodes and the solid electrolyte have also been studied [33, 37, 38]. The studies on the thin films range from typical PLD studies of the films as a function of deposition conditions to electrochemical studies, such as *in situ* scanning tunneling microscopy studies during cycling, to studies about the capacity, cycling stability, lithium-ion diffusion coefficients, or orientation [39]. Some examples are pure (LiCoO_2) and doped Li-cobaltate ($\text{LiCo}_{1-x}\text{Al}_x\text{O}_2$); additional Al_2O_3 coating on LiCoO_2 thin films; double layers of $\text{WO}_3(\text{V}_2\text{O}_5 \text{ doped})/\text{V}_2\text{O}_5(\text{TiO}_2 \text{ doped})$; $\text{Li}_x\text{V}_2\text{O}_5$ and Ag composite material, i.e. $\text{Li}_2\text{Ag}_{0.5}\text{V}_2\text{O}_5$; $\text{NiO-V}_2\text{O}_5$; $\text{Ta}_2\text{O}_5\text{-ZnO}$; anatase [33]; and LiFePO_4 in the form of thin films and as needle-like structures, which has been obtained by

off-axis PLD [40]. Some literature data are based on materials that are less common in the field of energy storage or conversion but are ideal for studying the mechanism of diffusion [41, 42].

The energy per footprint increases with the thickness of the cathode and anode electrodes. On the other side, an increasing of the electrode thickness will lead to power limitations due to a slow lithium-ion diffusion kinetic. In order to overcome these limitations, the compact and dense electrode material is replaced by a thick and porous film composite electrode film (Figure 5).

In state-of-the-art lithium-ion cells for HE applications, the electrodes, anodes, and cathodes are complex multi-material systems with defined material components, grain sizes, porosities, and pore size distributions in the micrometer and submicrometer range. Thick-film electrodes are formed from slurries/pastes of active material powders, binders, solvents, and additives (Figure 5) spread on current collector foils via tape casting, slot-die coating, or laser printing technologies [43, 44]. The materials are usually ground to a small particle size and fabricated into composite porous electrode structures with a polymer binder to give the film mechanical strength. Thick-film electrodes reveal a high porosity in the range of 30–50%, which in general enables a penetration of liquid electrolyte through the composite film down to the current collector. A liquid electrolyte contained in the pores enables ionic pathways, and a conductive additive, typically acetylene black, provides electronic pathways to the surfaces of the active material particles where the redox reaction occurs. The homogenous wetting of the complete electrode with liquid electrolyte is required for achieving a sufficient lithium-ion diffusion kinetic in the entire lithium-ion cell and to avoid enhanced degradation processes and hot spots during electrochemical cycling. Therefore, the wetting process is a key issue and also cost-intensive in battery manufacturing [26, 45]. Conventional LIBs found in applications have a typically single cathode film thickness of about $50 \mu\text{m}$ [26].

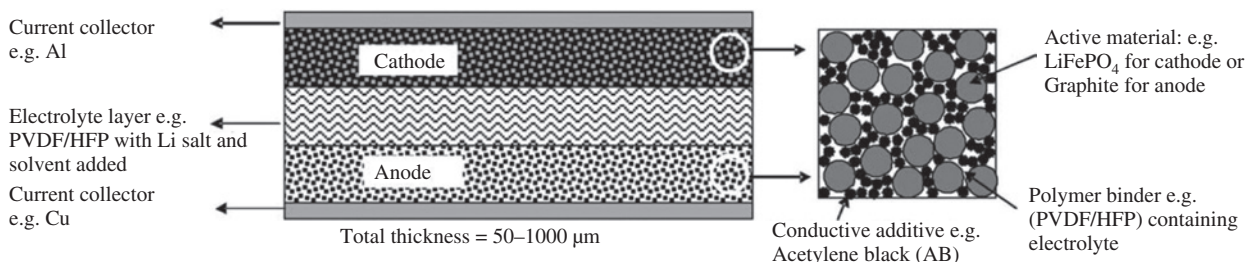


Figure 5: Schematic diagram of a thick-film cell. Reprinted from [28].

In commercial cells it is common to reduce binder and carbon black in electrodes in order to increase the energy density. This leads to a high amount of active material in the coating in the range of up to 96 wt%. Another approach is to further increase the film thickness of electrodes, which leads to a reduced amount of inactive material, namely, metallic current collector (aluminum for cathode, copper for anode) and separator material. A thicker cathode and anode would mean that for a given capacity, e.g. 52 Ah, the number of electrode and separator sheets would decrease. For battery production, fewer numbers of electrode sheet cutting and electrode sheet stacking steps would be required leading to an increased throughput and improved cost efficiency. For a 52 Ah cell, based on the technical data given in [26], the final cell weight and specific cell capacity

as a function of cathode film thickness was calculated (Figure 6), starting from the state-of-the-art cathode film thickness of 50 μm . For a cathode film thickness of 150 μm and 300 μm an increase in specific cell capacity can be achieved by 22% and 29%, respectively.

Obviously, thick-film LIBs (electrode thickness >100 μm) could achieve higher areal energy densities; the energy per footprint area increases with the thickness of the cathode; however, lithium-ion diffusion kinetics as well as the mechanical integrity of the film decreases with the thickness. The latter one is due to the fact that the active material expands and contracts during electrochemical cycling.

4 Laser cutting of electrodes

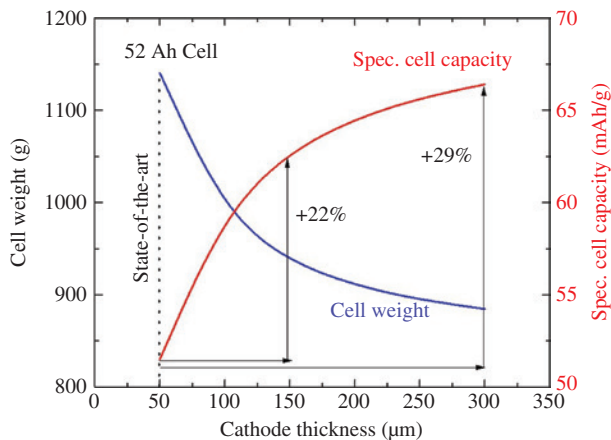


Figure 6: Impact of NMC cathode film thickness on cell weight and specific cell capacity (state-of-the-art 52 Ah cell: footprint area $21 \times 24 \text{ cm}^2$, cathode film thickness 50 μm , 37 double-sided cathodes, 36 double-sided anodes, 2 single-sided anodes, 39 separators, and 204 ml electrolyte [26]).

In general, the final contour of thick-film anodes and cathodes is achieved by punching of electrode sheets. Laser cutting might be an appropriate approach to replace the current technology due to the fact that mechanical blanking is associated with tool wear and inflexibility regarding cell and electrode design. It is assumed that a critical laser cutting speed of 1 m/s is necessary to be competitive with punching [46], which corresponds to cutting of one to two electrode sheets per second for HE cells (>20 Ah) with pouch cell design and conventional electrode film thickness of about 100–150 μm (total thickness of a double side coated electrode including current collector) [47, 48]. A typical NMC electrode sheet design for lithium-ion cells with pouch cell configuration is shown in Figure 7A–C. A vacuum chuck (Figure 7A) for appropriate sheet positioning and subsequent laser cutting (Figure 7B) is applied. Dust particles caused by the laser cutting are exhausted in order to avoid interaction with the incidence laser beam

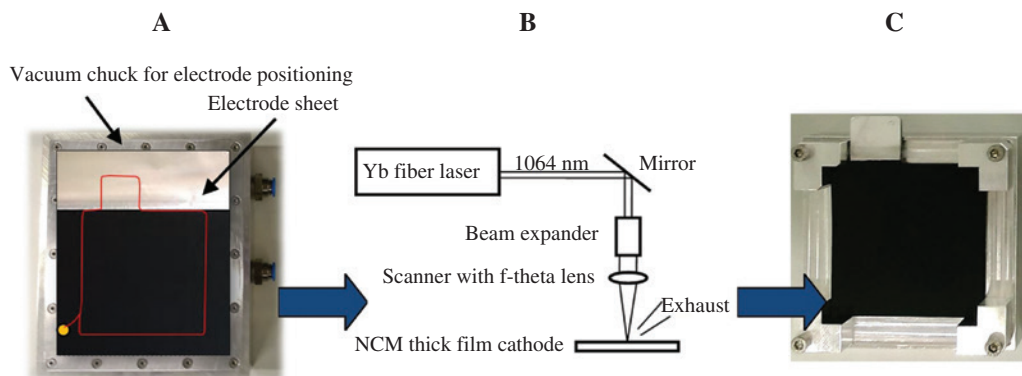


Figure 7: NMC cathode sheet before and after laser cutting (footprint area $8 \times 8 \text{ cm}^2$).

(A) vacuum chuck and electrode sheet. The red line describes the desired electrode contour; (B) schematic view of laser cutting of electrode sheets using scanner optics; (C) laser-cut electrode sheet in a storage box for subsequent assembly process.

and in order to reduce the number of particles on the final electrode surfaces (Figure 7C) and along the cutting kerf. Those contaminations and laser-induced material modification could be starting points for chemical degradation or lithium plating, which would have an impact on the overall battery lifetime.

Therefore, the cut edge quality has to be investigated in detail. For graphite anodes and NMC cathodes the laser cutting process by using cost-efficient nanosecond (ns)-laser technology is already presented in some battery manufacturing routes [49]. Due to different ablation thresholds of metallic current collector (copper or aluminum) and composite thick-film electrode coating and due to the Gaussian intensity laser beam profile, a characteristic cut edge geometry as described in [50–52] is achieved (Figure 8).

A step between the metallic current collector and the thick-film electrode is formed. The so-called “clearance width” has to be kept as small as possible, in general smaller than 50 μm . Figure 8 shows a laser cut edge of a graphite anode [52]. Typical defects caused by laser cutting are a heat-affected zone (HAZ) on both sides of the anode, burr along the cutting kerf, and the already mentioned clearance width. Even with optimized process parameters, ns-laser cutting will always induce a thermal impact to the electrode material. This is due to thermal diffusion length δ_w and surface temperature rise ΔT during laser processing, which is mainly controlled by laser parameters such as laser pulse duration τ and laser repetition rate v_{rep} . A short pulse duration maximizes the peak power and can reduce the thermal conduction to the surrounding material, which can be described by the thermal diffusion length

$$\delta_w = \sqrt{4\kappa \cdot \tau} \quad (2)$$

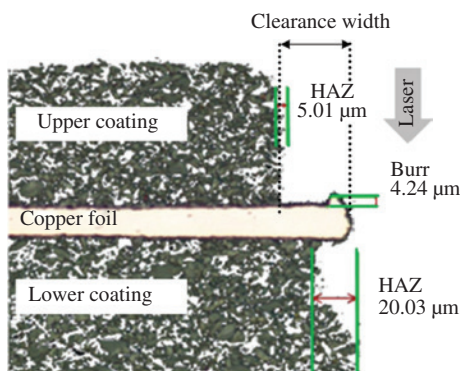


Figure 8: Cross-section view of an anode laser cut edge (laser scan speed 1200 mm/s, laser wavelength 1064 nm, average laser power 100 W). Reprinted from [52].

where κ [m^2/s] denotes the thermal diffusivity, which is about $\kappa = 1.5 \cdot 10^{-7} \text{ m}^2/\text{s}$ for composite NMC thick-film electrodes [53]. For a 200 ns laser, the thermal diffusion length achieves values of about 350 nm, while for 350 fs a value of smaller than 0.5 nm is obtained. Due to the fact that the primary particle size of active materials such as NMC is in the range of 50 nm up to a few hundreds of nanometers [54], the thermal diffusion length of ns-laser radiation might be already critical.

Heat accumulation and subsequent thermal damage of the material during laser processing is influenced by the laser repetition rate v_{rep} . If v_{rep} is too low, the energy loss by heat conduction dominates, and all of the energy not used for ablation will leave the ablation zone. Higher repetition rates lead to an increase of the average surface temperature ΔT , which can be estimated by solving the one-dimensional heat equation for a rectangular laser pulse [55]

$$\Delta T = 2(1-R) \cdot \varepsilon \cdot v_{\text{rep}} \sqrt{\frac{t}{\rho c_p K \pi}} \quad (3)$$

where R is the reflectance, t the laser processing time [s], ρ the density [g/cm^3], c_p the specific heat capacity [$\text{J}/(\text{g K})$], and K the thermal conductivity [$\text{W}/(\text{cm K})$]. The local temperature increases linearly with the repetition rate, and even with femtosecond (fs)-laser radiation, values of about $\Delta T = 7000^\circ\text{C}$ can be reached by using 1 MHz laser repetition rate and an accumulation of 20 laser pulses [56]. A higher surface temperature in turn can induce an increase of the material quantity removed per laser pulse. This can make the cutting process more efficient. Nevertheless, a thermal damage of the electrode material or melt and debris formation should be avoided.

The laser-material interaction is a complex combination of photochemical and photothermal processes and is dependent on the laser characteristics and materials' properties. The dominating laser beam absorption mechanisms may be either single-photon or multiphoton processes. A single-photon absorption process is characteristic for material ablation using UV laser radiation and ns-laser pulses. While multi-photon absorption processes play an important role by the use of ultrashort laser pulses with pulse length τ in the picosecond ($\tau < 10 \text{ ps}$) and femtosecond (10^{-15} s) range. In the case of fs-laser pulses, the high intensity delivered by the focused laser beam can induce strong nonlinear optical absorption of photons in materials that might otherwise be highly transparent to photons at much lower intensities. Another advantage is the reduction of residual damage by minimizing thermal effects [57–59].

Besides the above mentioned laser-induced defects, also a chemical modification by material re-deposition

could happen. It was detected by chemical analysis applying TOF-SIMS (time-of-flight secondary ion mass spectrometry) that due to ns-laser cutting of thick-film graphite anode sheets, a thin copper contamination layer was deposited on the upper coating of the electrode (Figure 9A), which is due to evaporation of copper from the current collector during the cutting process.

It is obvious that by applying fs-laser radiation the amount of metallic contamination on top of the electrode can significantly be reduced (Figure 9B). Furthermore, during fs-laser cutting, the formation of a step between the metallic current collector and the thick-film electrode, which is characteristic for ns-laser cutting (Figure 9C), can be completely avoided; i.e. the clearance width can be decreased down to 0 (Figure 9D). If ns-laser cutting of anodes can lead to deposition of a very thin copper film on top of the electrode, then it could be expected that along the cutting kerf a similar contamination would be formed. This was simulated and investigated experimentally for laser cutting of single-side coated graphite anodes by using a high-power (500 W) continuous wave fiber laser operating at a wavelength of 1060 nm [61]. In Figure 10A, the side view of a laser-cut graphite anode, 90 μm in thickness, is

shown. A good cut edge quality is achieved, and the characteristic clearance width is presented without delamination, crack formation, edge banding, burrs, or visible debris formation along the sidewall. Melt formation along the copper current collector can be detected, which is due to re-solidification. Lee et al. [61] developed a 3D mathematical model for high-speed laser cutting of graphite anode material with which a theoretical copper concentration profile along the cutting kerf could be achieved (Figure 10B). The copper concentration along the cross section of the laser-cut graphite layer was also measured by using energy-dispersive X-ray spectroscopy (EDX) and compared with the simulation results (Figure 10C). Most of the graphite anode cross section showed a copper concentration smaller than 10%. At 20 μm above the interface of copper foil and graphite layer, the copper contamination increases significantly up to values of almost 100%.

Continuous wave, long pulse, or ns-laser cutting of graphite anodes are in general not critical regarding process integration in battery manufacturing. A marginal copper contamination seems to have no negative impact on battery performance. Furthermore, short-pulsed laser sources are so far preferred in industry in comparison to

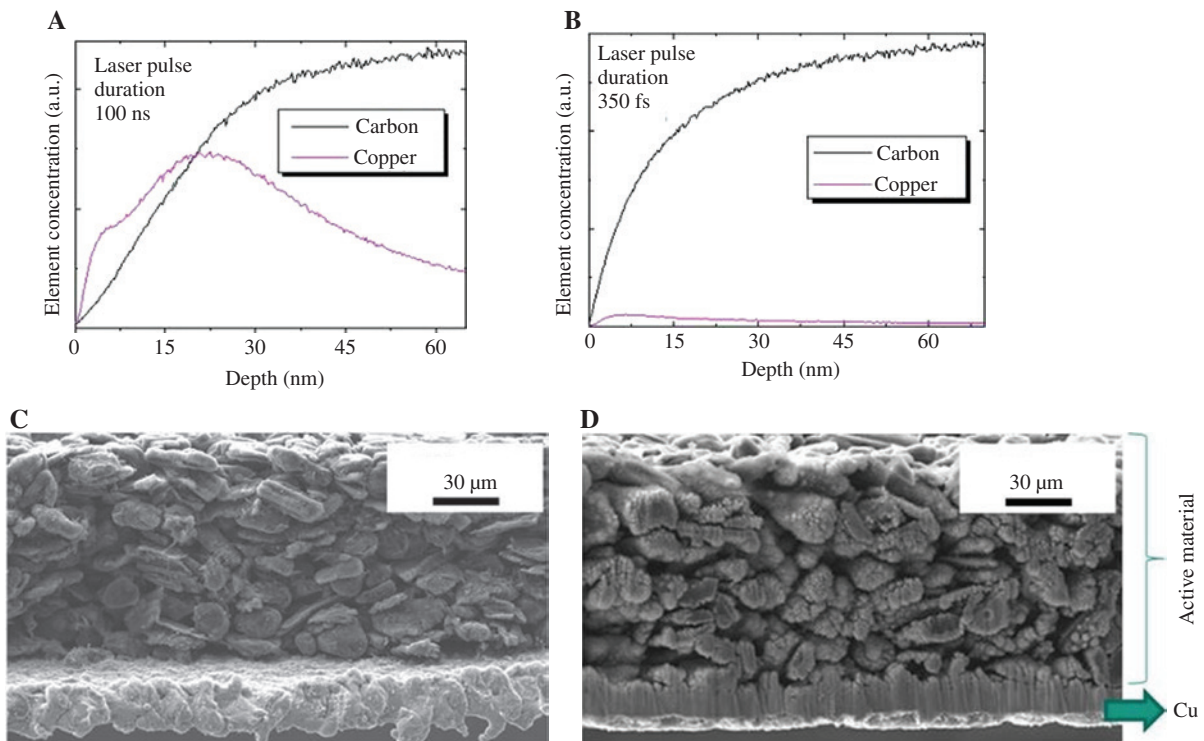


Figure 9: Laser cutting of single-side coated graphite anode.

(A, B) TOF-SIMS depth profile close to the cut edge on top of the electrode layer: (A) cutting with ns-laser radiation (pulse length 100 ns and (B) cutting with ultrafast laser radiation (pulse length 350 fs). (C, D) SEM image of cut edges produced by (C) ns-laser radiation (100 ns) and (D) by ultrafast laser radiation. Reprinted from [60].

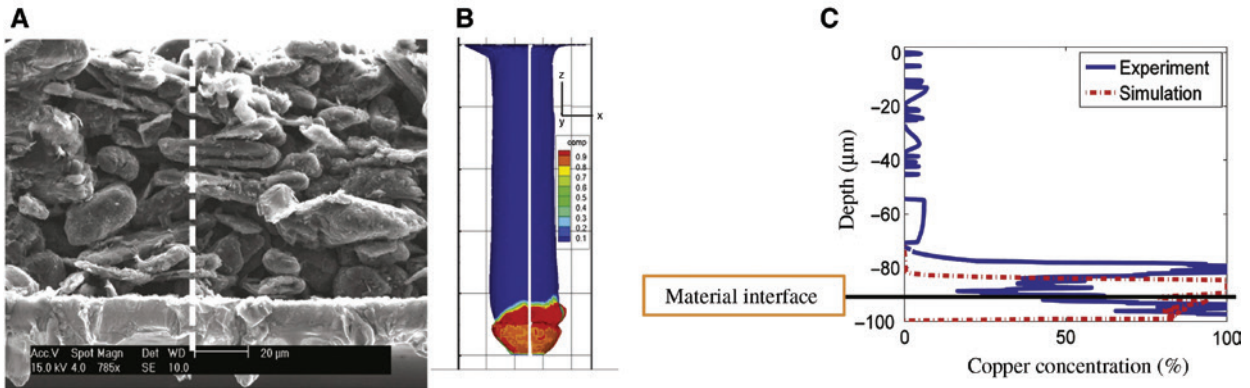


Figure 10: Copper deposition along laser cut graphite anode.

(A) SEM image of laser cut anode in cross-section view; (B) copper elemental mapping along cutting kerf (simulation) and (C) comparison of the copper concentration between experiment and simulation. Reprinted from [61].

ultrafast laser systems due to the fact that ns-laser systems with significantly higher laser power and lower investment cost are available. Nevertheless, the recent development of high-power ultrafast laser is an emerging topic, which might get relevance for industrial applications in the near future. Related to ultrafast laser radiation for high volume materials processing in industrial applications, the further development of optical devices with improved lifetime and fast scanner systems for handling of high repetition rates is absolutely required.

There are other types of electrodes that undergo chemical modifications or phase change during thermal-driven laser processing. This could lead to significant drawbacks in cell lifetime or cell capacity. For example, LFP electrodes tend to form droplet-like particles in the HAZ which is produced during laser cutting. Those particles are sticking at the cutting kerf [62]. Given the complex behavior of LFP, several different phases may exist at room and higher temperatures. With heating, olivine LiFePO_4 in the cathode may oxidize to form $\alpha\text{-Fe}_2\text{O}_3$ or may undergo microstructural modification to form $\gamma\text{-Li}_3\text{Fe}_2(\text{PO}_4)_3$ [63, 64]. Lutey et al. [62, 63] investigated laser cutting of LiFePO_4 and NMC and tried to find the best condition of processing efficiency. Nevertheless, in order to avoid microstructural and chemical changes along the cut edge, the use of ultrafast laser radiation may be the right choice.

5 Laser annealing and drying of electrodes

Laser-assisted thermal treatment of active material for lithium-ion cells can be applied for thin and thick-film

electrodes. The as-deposited thin-film material has in general not the proper crystalline battery phase and chemical composition. Therefore, rapid laser annealing can replace long-term conventional oven processes in order to tune the material properties. For thick composite films the chemical composition and crystalline phase are already provided in the desired form. Nevertheless, attached to the particles and the binder material, water and solvent act as critical contamination which has to be removed prior to cell assembly and electrolyte filling process. A drying process, normally realized by time- and energy-consuming oven processes, could be in future an economic laser-driven technology. Both approaches will be presented in this section.

5.1 Laser annealing of electrodes

Rapid annealing processes for LMO thin-film electrodes have already been applied by using halogen lamps for so-called rapid thermal annealing [65–69]. The annealing processes can improve the microstructure of the films, but many cracks may be easily formed in the process due to volume expansion and shrinkage. Large area thermal treatment can also reduce the flexibility to combine materials; e.g. the use of flexible and low-temperature materials as substrates will become critical. Laser annealing could be, for example, locally applied only on the desired electrode material. Laser annealing has already been widely applied to crystallization of amorphous semiconductor materials, like amorphous silicon, which are deposited on different types of substrates such as glass or polymers [70]. Laser annealing could be also a powerful tool for control of crystalline phases in cathode thin films, and

regarding the industrial established thin-film transistor laser annealing also an up-scaling for application seems to be possible. And indeed, rapid laser annealing was already successfully established for crystallization of thin cathodes such as LiCoO_2 or LiMn_2O_4 [71–74]. Besides the crystalline phase also, the grain size could be controlled for LiCoO_2 and LiMn_2O_4 thin films as a function of annealing time. In case of LiCoO_2 it was shown that suitable annealing temperatures are in the range of $T = 400\text{--}700^\circ\text{C}$. Temperatures lower than or equal to 400°C led to an insufficient phase conversion, while temperatures equal to or above 700°C led to the formation of a contamination phase (Co_3O_4). High-power diode laser annealing processes were also developed for rf magnetron sputtered lithium manganese oxide thin films with the aim to form a spinel-like phase [75]. The Raman spectrum for an as-deposited Li-Mn-O thin-film is depicted in Figure 11B (1). Applying an annealing temperature of $T = 600^\circ\text{C}$ for $t = 100$ s on the film, significant changes within the Raman spectra could be observed [Figure 11C (1)]. The characteristic peaks for the electrochemically inactive Li_2MnO_3 phase could be assigned [76, 77]. With an increase in laser annealing temperature up to $T = 680^\circ\text{C}$ and a fixed annealing time of $t = 100$ s [Figure 11D (1)], Raman spectroscopy indicates a spinel-like Li-Mn-O phase showing the typical bands which indicate stretching vibrations of manganese and oxygen compounds at 629 cm^{-1} (A_{1g} species), the shoulder around $\sim 590\text{ cm}^{-1}$ (F_{2g}), and a weak band at 482 cm^{-1} (F_{2g} species) [76, 78].

Similar Raman spectra could be observed for an annealing temperature of $T = 600^\circ\text{C}$ by applying an

annealing time of $t = 2000$ s [Figure 11E, (1)]. The thin films showing the spinel phase were cycled and analyzed with respect to the composition of the formed solid state interface (SEI) layer [75]. Cyclic voltammogram scans identified that film annealing at $T = 600^\circ\text{C}$ for $t = 2000$ s leads to characteristic redox peaks for spinel thin films [Figure 11, (2)].

5.2 Drying of thick-film electrodes

As described in Section 3, thick-film electrodes are manufactured from slurries of active material powders, binders, solvents, and conductive agents and further additives. As shown in Figure 12, the viscous slurry can be homogeneously distributed along the current collector by tape casting or slot die coating. The significant amount of solvent leads to a shiny surface after the coating process. The wet coating usually is dried with hot air or with thermal radiation and subsequently calendered to a specific porosity. After that, the surface becomes optically matte. The drying process of wet composite thick electrode films is an important step in cell manufacturing. For example, film adhesion is mainly influenced by the drying process, which was investigated by Günther et al. [79]. It was shown that rapid drying by using large area infrared dryer can lead to a separation of the active particles and the NMP (N-methyl-2-pyrrolidone) or water-soluble binder, affecting the adhesion and cohesion strength of the electrode. It was also shown that cells made from electrodes with good film adhesion show also a higher cell capacity. Besides improving the mechanical

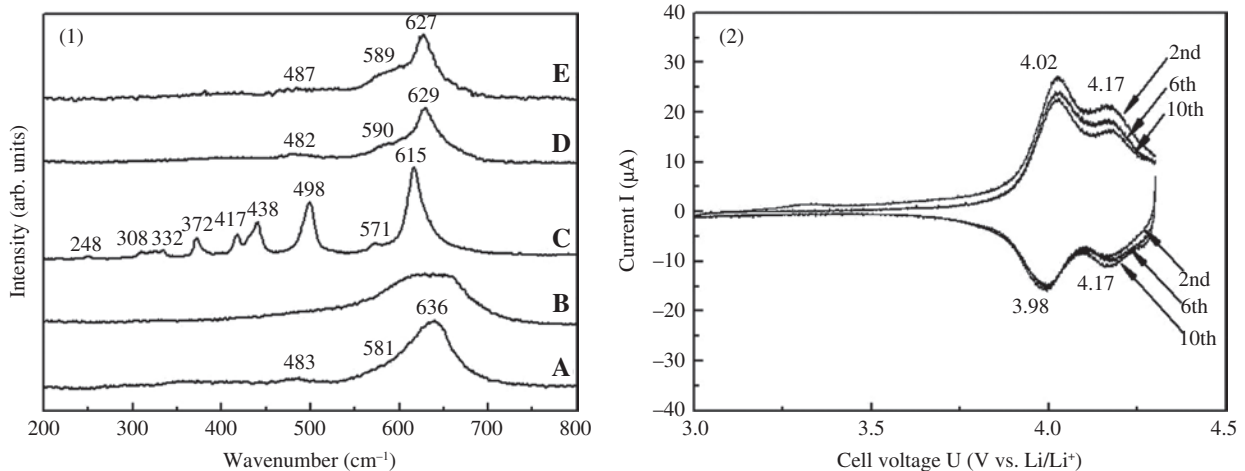


Figure 11: Effect of high-power diode laser annealing on crystallinity and electrochemical performance: (1) Raman spectra of $\text{Li}_{0.88}\text{Mn}_{1.98}\text{O}_4$ thin films (B–E) and LiMn_2O_4 reference powder (A), as-deposited film (B), laser annealing was performed for $t = 100$ s at $T = 600^\circ\text{C}$ (C), for $t = 100$ s at $T = 680^\circ\text{C}$ (D), and for $t = 2000$ s at $T = 600^\circ\text{C}$ under ambient air (E); (2) cyclic voltammograms ($\text{Li}_{0.88}\text{Mn}_{1.98}\text{O}_4$, laser annealed for $t = 2000$ s at $T = 600^\circ\text{C}$). Reprinted from [75].

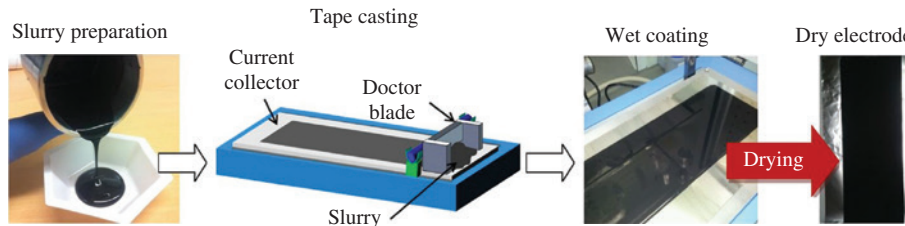


Figure 12: Processing steps for thick-film coating of composite cathode materials via tape casting.

stability of the coating, the removal or residual moisture in electrodes is per se crucial for achieving the desired electrochemical performance which was recently investigated in detail for cathodes made of NMC-532 ($\text{LiNi}_{0.5}\text{Mn}_{0.3}\text{Co}_{0.2}\text{O}_2$) by Li et al. [80]. Drying of electrodes has also an economic aspect and shows great energy-saving potential. For a single 52 Ah pouch cell it was calculated by Wood et al. [26] that an energy consumption of 31.5 kWh would be required to remove 709.8 g NMP solvent by hot air drying.

With respect to the economic aspect, Vedder et al. [81] and Hawelka [82] recently developed laser-based drying technologies for anode (graphite) and cathode (LFP) for LIBs. The principal experimental setup is shown in Figure 13. For this purpose, a fiber laser (450 W maximum average power) operating at a wavelength of 1070 nm was applied. It could be proven that the electrochemical performance, the residual moisture, and the electrode morphology are almost the same for electrodes, which were dried by laser and by a conventional oven process. Peel-off tests were performed, and one can conclude that the film adhesion to the current collector foil for both types of electrodes shows no differences. The laser radiation is absorbed directly in the wet coating, and ambient heat losses can be kept small. In comparison to the oven

process, the laser process could reduce the energy consumption for drying by a factor of 2. Nevertheless, up to now, the laser process could reach processing speeds of only $50 \text{ cm}^2/\text{s}$. For typical coating speeds of 30 m/min for 52 Ah cells (footprint area $21 \times 24 \text{ cm}^2$) a laser processing speed of about $1050 \text{ cm}^2/\text{s}$ would be required. Further process upscaling using high-power lasers and further process optimization will be necessary.

6 3D battery concept

The development of 3D electrode architectures in LIBs is a relatively new approach for overcoming the problems related to a restricted battery performance, e.g. power losses or high interelectrode ohmic resistances [16, 18], and mechanical degradation during battery operation due to high volume changes resulting from lithium-ion insertion [20]. The general strategy is to design cell structures that maximize power and energy density yet maintain short ion transport distances. A 3D matrix of electrodes is proposed in order to meet short transport lengths and large energy capacities in comparison to conventional 2D electrode designs (Figure 14A and B) [16]. In the recent concept [85–87], the 3D micro-battery based on micro- and nano-structured architectures could potentially double the energy density by fully utilizing the limited space available. The manufacturing process for 3D architectures is usually a subtractive manufacturing. A common approach is 3D structuring of the electrode substrate, the current collector, before deposition of the thin-film electrode. Baggetto et al. [84] and Xie et al. [88] adopted an approach which aligned well with state-of-the-art integrated circuit technology such as standard lithography, etching technologies and thin-film deposition (Figure 14C). For this purpose, they used silicon as substrate for the so-called 3D-integrated all-solid-state battery.

All of these researches prove that 3D patterning of electrodes improves the electron and ion diffusion kinetics in the electrodes. Unfortunately, these methods are in

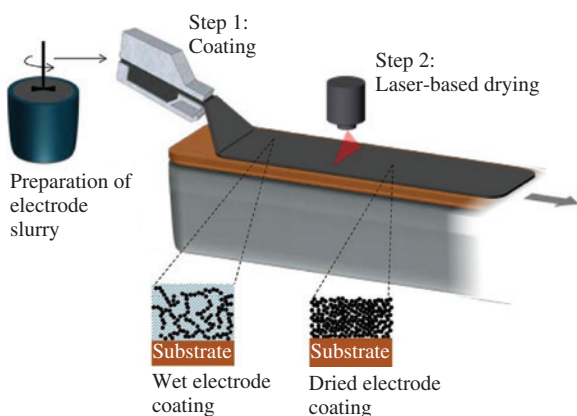


Figure 13: Process chain for the production of thick-film electrodes. For the drying process, the wet electrode is exposed to the line focus of a high-power fiber laser. Reprinted from [81].

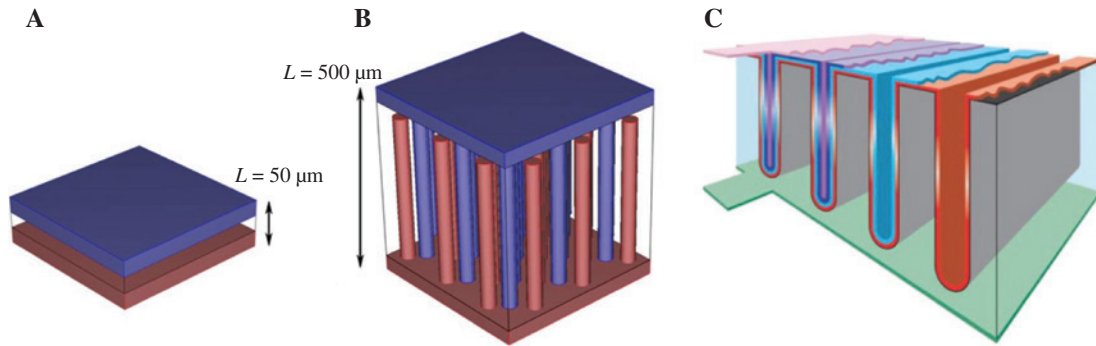


Figure 14: Concepts for electrode designs and arrangements suggested for micro-battery applications. Schematic view of (A) 2D and (B) 3D electrodes [83] and (C) an all solid state lithium-ion micro-battery integrated in a 3D substrate [84].

a very early stage of development and normally applied for model electrodes in thin-film micro-batteries. Furthermore, it is generally not feasible for up-scaling to thick-film composite electrodes or for large electrode footprint areas.

Laser manufacturing of 3D lithium-ion thin- and thick-film batteries was realized also by direct structuring of the active material [14, 75, 89, 90]. With the electrode fabricated by laser ablation or modification, the 3D and high aspect ratio battery was completed. The laser-engineering structured electrode provides a significant improvement of cycle retention, and an increased power density and energy density on cell level could be achieved. The principle approach is shown schematically in Figure 15.

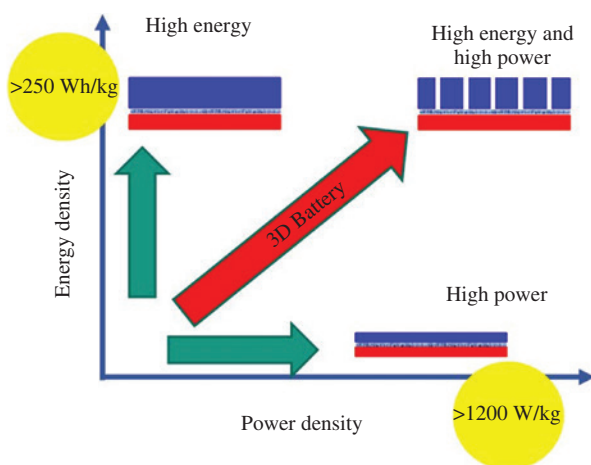


Figure 15: Schematic view of energy density as a function of power density for 2D, 3D, and thick-film electrodes (red: current collector of the electrode; blue: active material of the electrode). The yellow marked values of energy density and power density are related to target values on cell level for the year 2025 based on [4].

6.1 Structuring of current collectors

Mechanical and chemical degradation processes in LIB operation are rather complex and are mainly responsible for a short battery lifetime. During charging and discharging, the electrodes of a battery undergo a volume change due to intercalation and de-intercalation of lithium-ions. Graphite anodes with a practical capacity of about 330 mAh/g are used in state-of-the-art LIBs, and they exhibit 10% volume expansion under charge [91]. Tin oxide, silicon, or silicon-doped graphite have been regarded as the most promising anode materials for next-generation LIBs [92]. This is due to the fact that tin oxide and silicon can theoretically enable a lithium uptake that is almost 10 times higher than that of graphite. The large number of lithium-ion insertion/extraction results in huge volume change of up to 400% [15, 20, 93]. In general, the huge change in volume leads to the formation of cracks, pulverization of the electrode, and film delamination combined with a subsequent reduction of available active material due to loss of electrical contact. Furthermore, cracks are starting points for chemical degradation due to interaction of the electrolyte with the active material. This continuing SEI formation leads finally to a reduction of battery active material. A significant increase of adhesion forces between the anode composite layer and the current collector would lead to an improvement of mechanical stability and capacity retention and lifetime, which was shown in a rather new approach by Tang et al. [15]. They could reveal that blind holes of 50–100 μm diameter and an aspect ratio of 1 (Figure 16B) which were laser generated in copper plates (Figure 16A) with a thickness of 150 μm can act as mechanical anchoring for silicon-based active coating leading to a significant improvement of battery cycle retention (Figure 16C and D). It should be pointed out that state-of-the-art HE batteries use current collector foils with thicknesses in the range of 6–20 μm.

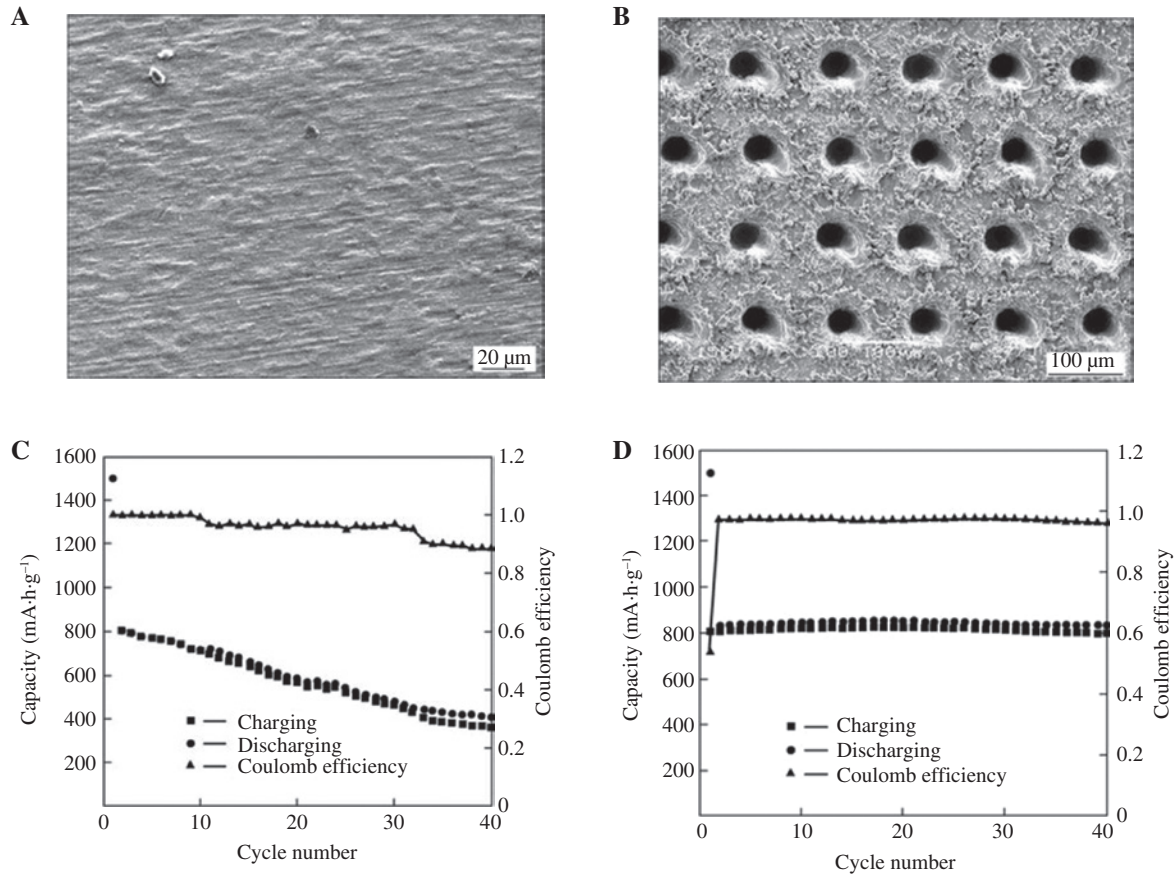


Figure 16: Impact of laser-drilled current collector plate on cell performance: (C, D) specific capacity and coulomb efficiency of silicon-based anodes deposited on (A) unstructured and (B) laser-drilled copper plates (A, B: SEM images, copper plates: 150 µm in thickness). Reprinted from [15].

The coulombic efficiency of a battery is the ratio of charge capacity divided by the following discharge capacity. High coulombic efficiency means that low battery losses are given.

A transfer of the above mentioned approach into battery manufacturing needs a significant down-scaling of structure sizes and depths as shown by the following methods: laser printing combined with wet chemical etching of Cu and subsequent Si thin-film deposition [94], and laser drilling of porous graphite anode films [95] were recently successfully applied in order to improve the electrochemical performance of anode materials in micro-batteries. Zhang et al. [96] could improve the anode film adhesion on thin Cu foils by introducing ultrafast laser micro-/nano-structuring prior to anode coating process. They could reveal that a periodic pattern by single pulse fs-laser ablation induces a self-organized nano-structuring which is very similar to the so-called laser-induced periodical surface structuring leading to a hierarchical surface pattern on thin-film current collectors made of copper or aluminum [97]. Additionally to an improved film adhesion, a reduction of impedance and a higher cycle lifetime was detected. It is assumed that the

improved lithium-ion diffusion is induced by a preferred orientation of the graphite particles along the micro-/nano-structured Cu surface.

6.2 3D electrode architectures

Different types of laser processing for increasing the active surface area were established, i.e. “laser-assisted self-organizing structuring” and “direct structuring” of electrodes. The first of these processes can be applied to thin-film and thick-film electrodes that have small electrode footprint areas, e.g. for coin cells. The second process is not limited to micro-batteries like for other technical approaches listed in [19], which means that the 3D battery concept can be also applied for large electrode footprint areas, such as for HE pouch cells.

The formation of self-organized surface structures (Figure 17A) on LiCoO₂ and Li(NiMnCo)₂ (NMC) thick- and

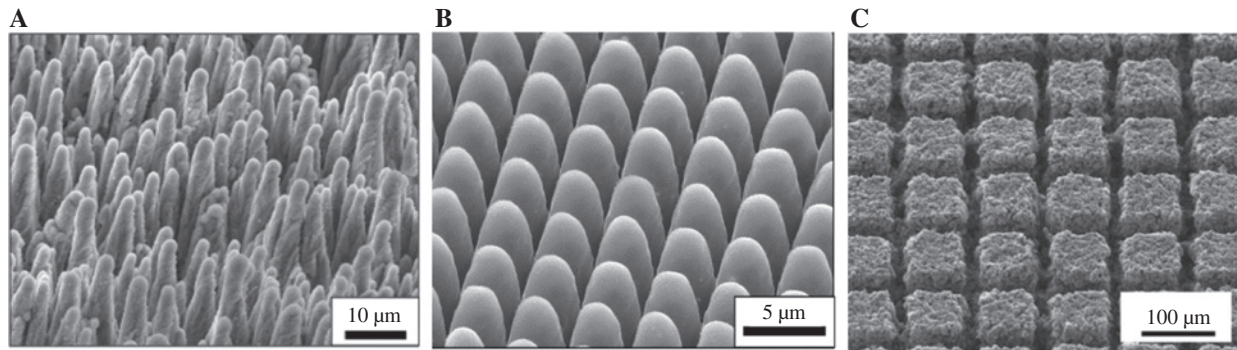


Figure 17: SEM image of microstructures laser-generated in electrode cathode materials: (A) self-organized microstructures in LCO composite electrodes by excimer laser exposure, (B) direct excimer laser micropatterning of thin-film LCO electrodes, and (C) micro-pillars in composite LCO electrode obtained by direct fs-laser structuring.

thin-film electrodes was achieved by excimer laser ablation at 248 nm wavelength. The self-organized structuring process [10, 72, 98] can be explained by selective material ablation and subsequent material re-deposition. It was possible to avoid material loss during laser patterning. The active surface area can be increased by a factor of about 10. Also, direct excimer laser ablation of thin-film LCO electrodes with structure sizes in the micrometer range could be realized with high surface quality (Figure 17B). Nevertheless, the processing speed using excimer laser sources with an average power of 10–20 W is quite low, so that it is proposed to apply this technology for micro-batteries with small footprint area. For high processing speeds and HE cells with large footprint area, direct laser structuring, either with ns fiber lasers (e.g. 200 ns) or fs-lasers (e.g. 380 fs) (Figure 17C), was established for realizing 3D microstructures.

Thick-film LIBs (electrode thickness $>100 \mu\text{m}$) could achieve high areal energy densities; the energy per footprint area increases with the thickness of the cathode. On the other side, for thick-film cathodes, the supply of lithium-ions and therefore the diffusion kinetics, especially at high charging/discharging rates, becomes limited in those parts of the electrode that are closer to the current collector, and a lithium concentration gradient along the film thickness will be established. This is worse with increasing film thickness. Therefore, not all lithium-ions of the active material can take part in lithiation/de-lithiation processes leading to a drop in capacity. This capacity drop is already observed for low charging/discharging currents of “C/2”, which was reported for the performance of an optimized pair of conventional lithium-ion anode and NMC cathode with single-sided thicknesses of each $320 \mu\text{m}$ [99]. “C/2” means that the time for charging and discharging takes 2 h each. Additionally, the mechanical integrity of the film decreases with the

thickness, as the active material expands and contracts during cycling.

The thick-film concept provides HE cells, while high-power application and mechanical relaxation become possible by introducing the 3D battery concept. State-of-the-art high-power LIBs are usually achieved through a “thin-film” concept or by 3D electrode architectures with improved interfacial kinetics. However, due to manufacturing constraints, the thin-film and 3D technologies are limited to micro-batteries for niche applications. The combination of both concepts – 3D battery concept and thick-film concept – will realize a battery system with high power and high energy at the same time (Figure 15).

Thick films made of NMC ($\text{LiNi}_{1/3}\text{Mn}_{1/3}\text{Co}_{1/3}\text{O}_2$) with thickness of $155 \mu\text{m}$, $185 \mu\text{m}$, and $210 \mu\text{m}$ were produced by tape casting. The coating process is described in [100]. Those coatings are beyond the state-of-the-art LIBs with a typical film thickness of $50 \mu\text{m}$. An increase of cathode film thickness from $50 \mu\text{m}$ up to $210 \mu\text{m}$ means that on 52 Ah cell level the energy density could be increased by 26% (Figure 6). Ultrafast laser ablation was performed in order to realize a periodic line pattern with a line-to-line distance of $200 \mu\text{m}$ [101] (Figure 18).

The electrochemical performance of LIB with laser-structured thick-film NMC electrodes was analyzed (Figure 19) for different C-rates, e.g. C/2 or 2C means that battery discharging takes 2 h or 30 min, respectively. Cells with unstructured thick-film electrodes reveal a strong decrease in capacity with increasing discharging current. With increasing film thickness, the specific discharge capacity of cells with unstructured electrodes decreases, even for low C-Rates. For C/5 the specific capacity for cells with unstructured films with a thickness of $155 \mu\text{m}$, $185 \mu\text{m}$, and $210 \mu\text{m}$ drops down to 132mAh/g , 111mAh/g , and 76mAh/g , respectively. Due to laser structuring of cathodes with $210 \mu\text{m}$ in film thickness, a loss in active

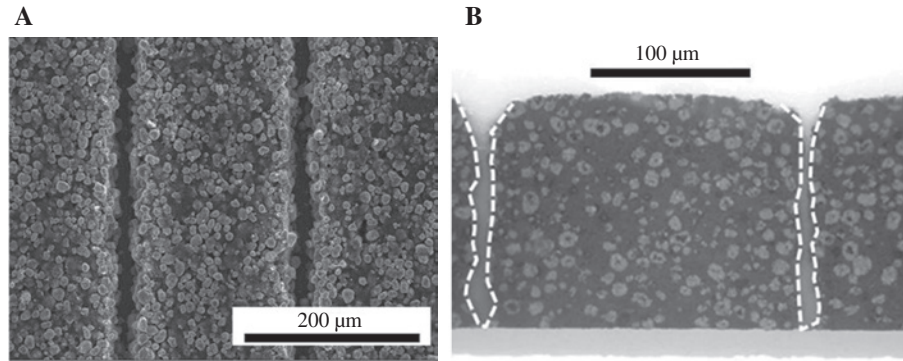


Figure 18: Laser structuring of NMC thick-film electrodes. (A) SEM image (top view) and (B) microscopy image (cross-section view) (film thickness: 155 μm).

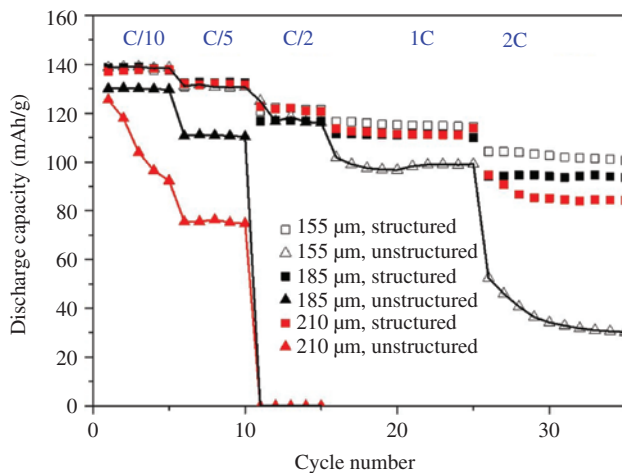


Figure 19: Specific discharge capacity as a function of cycle number for lithium-ion cells with structured and unstructured NMC-111 thick-film electrodes (film thickness: 155 μm, 185 μm, 210 μm) for different discharge C-rates.

material of 7% was obtained. On the other side, due to laser structuring, the specific capacity of cells with 210 μm cathode films can be increased by 74% for C/5. This is a huge effect, which cannot be explained by the small amount of active material removed during structuring. The main driven mechanism is the improved lithium-ion diffusion kinetics in 3D electrodes. For cells with structured electrodes cell failure at high C-rates can be avoided. Even for 2C, remarkable capacity retention for all film thicknesses could be achieved. That means that HE and high-power LIB become possible at the same time.

In recent research from Mangang et al. [102] it could be proven that the laser micro-structuring of thick-film LFP electrodes leads to an increase of the chemical diffusion coefficient, i.e. the lithium-ion diffusion kinetics could be significantly improved by increasing the active surface area due to laser structuring. It could be shown by Smyrek

et al. [103] that for laser-structured NMC electrodes the lithium concentration significantly increases along the contour of 3D microstructures (Figure 20), especially for high charging and discharging rates. It is stated that 3D architectures act as an attractor for lithium-ions, and a boost of battery performance regarding battery power and lifetime can be achieved.

Besides an improved lithium-ion diffusion kinetic in 3D electrode materials [20, 72, 73, 104–109], it has been shown that 3D grid structures can counter delamination from the current collector due to volume expansion during electrochemical cycling for both LMO intercalation cathodes and conversion-type tin oxide (SnO_2) anodes [20, 104]. Besides reduction of mechanical degradation of the electrode materials, chemical degradation and dissolution of active material components in the electrolyte has been influenced by laser processing into 3D conical microstructures and subsequent passivation by C-60 coating [89]. Finally, it could be shown that the cycling behavior of lithium manganese oxides in liquid electrolyte could be stabilized by passivation of 3D microstructures with indium tin oxide (ITO) thin films [105].

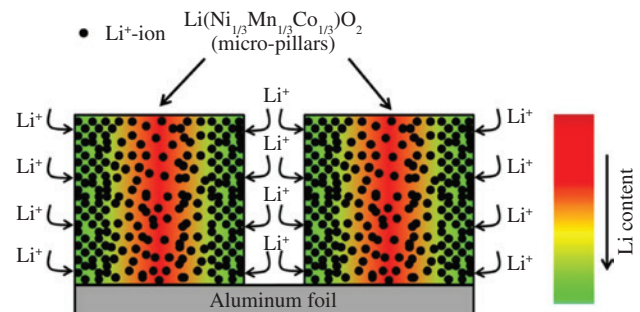


Figure 20: Schematic illustration for laser-structured NMC electrodes (in cross-section view) during electrochemical cycling at high discharge rates. Reprinted from [103].

One important issue is the loss in active material due to direct laser structuring of thick-film electrodes. The removal of active material depends on the pitch distance and on the type of laser ablation. By using 200 ns-laser radiation and a pitch distance of 200 μm , the loss in active material can reach values of about 30% [13] which is quite too high for industrial application. A pitch distance of 600 μm would reduce the material loss below 10 wt% while maintaining an improved wetting of the electrodes with liquid electrolyte (Section 6.4). Nevertheless, it is expected that an increasing pitch distance will reduce the lithium-ion diffusion kinetic and its impact on high rate capability. By using fs-laser ablation and the same optical beam path as for ns-laser radiation [13], higher aspect ratios and a reduced mass loss can be achieved in comparison to ns-laser ablation. For a pitch distance of 200 μm and a pulse length of 380 fs the loss in active mass could be reduced down to 6.8 wt% (Figure 18A and B). By increasing the pitch distance up to 300 μm , the loss in active material could be reduced down to 4.5 wt%.

The removal of active material will have an impact on the cell manufacturing costs. Figure 21 shows the cost contributions for production of a 52 Ah lithium-ion cell [26]. The total cell manufacturing costs are 272 \$/kWh, while 30% (82.5 \$/kWh) of these costs are attributed to the cathode material. For this state-of-the-art cell system, the cathodes are made of NMC with a layer thickness of 50 μm . It is assumed that the laser structuring process for such thin layers will lead to an active material loss in the range of 4–5% with a line pitch distance in the range of 200–300 μm . This means that due to active material removal

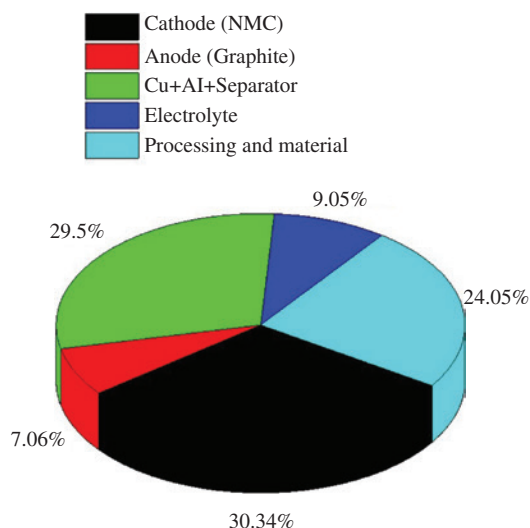


Figure 21: Cost contributions for state-of-the-art NMC lithium-ion cell manufacturing (cell manufacturing cost 272 \$/kWh; data were extracted from [26]).

additional costs for active material are in the order of 3.3–4.1 \$/kWh, which corresponds to an increase of cell costs in the order of 1.2–1.5%. This increase in cell costs will be overcompensated by the benefit of combining the 3D battery concept and the thick-film concept (Figure 6), which will be discussed in Section 6.4. Nevertheless, ongoing studies have to investigate in more detail the electrochemical performance as a function of pitch distance and material loss in order to find the most cost-efficient electrode design for high-power and HE applications.

6.3 Laser printing of batteries

For the fabrication of thick-film electrodes with small lateral resolution, printing technologies such as laser-induced forward transfer (LIFT) are appropriate and even suitable for the manufacturing of a complete all-solid-state lithium-ion micro-batteries [44]. LIFT has shown to be a promising method for fabricating lithium-ion micro-battery electrodes and even all-solid micro-batteries [110, 111]. LIFT is a direct write technique that allows printing from a variety of functional materials, such as composite electrode materials. It is a non-contact, nozzle-free additive manufacturing process for producing highly porous thick-film electrodes with adjustable thickness. While thin-film electrodes are in general made of compact thin films produced by physical vapor deposition or CVD processes with a film thickness in the micrometer range or less, laser printing of composite electrodes leads to minimum film thicknesses in the range of 5 μm . Due to multiple printing steps, one can adjust the electrode film thicknesses significantly above 100 μm [44]. Discharge capacities of about 2.6 mAh/cm² could be achieved for printed LiCoO₂ cathodes which is over an order of magnitude higher than those that were reported for sputter-deposited thin-film electrodes [44]. One of the advantages of LIFT is that the printed electrodes show porous structures with high active surface area. The porosity of such films can be in the range of 30–50% leading to an increased contact area between the electrodes and the electrolyte. The charge transfer will be significantly improved in comparison to dense and compact films, which is quite important for electrochemical devices.

LIFT for printing of batteries uses in general a pulsed UV laser [wavelength $\lambda = 355$ nm, pulse length (FWHM) $\tau = 30$ ns] beam to induce the transfer of nano paste material from a donor substrate (glass slide) onto a receiver substrate (Figure 22). The substrate (current collector) is facing the donor substrate at a distance of about 100 μm . When the laser intensity is higher than the threshold

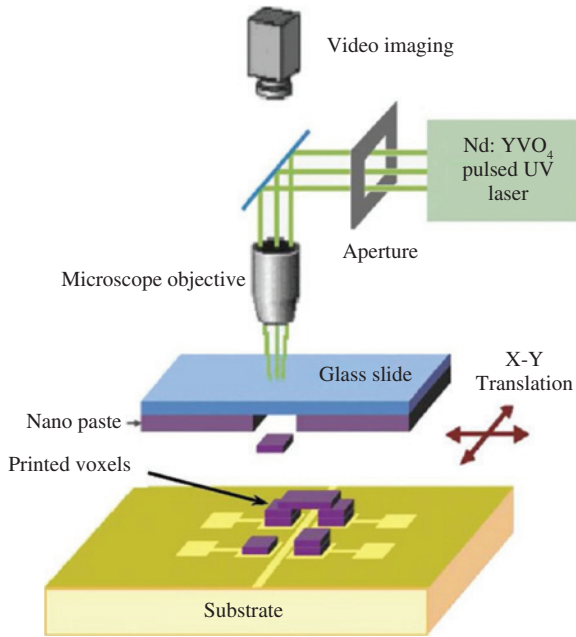


Figure 22: Schematic view of the LIFT setup. Reprinted from [112].

energy, material is ejected from the glass slide and is transferred to the substrate (“printed voxel”). For example, for printing of LiMn_2O_4 electrodes the laser intensity was maintained at $50 \text{ mJ}/\text{cm}^2$ [11].

Complete lithium-ion micro-batteries with LiCoO_2 as cathode and carbon as counter electrode were fabricated by LIFT, whereby the laser-printed electrodes were separated by a porous membrane (Figure 23). However, little

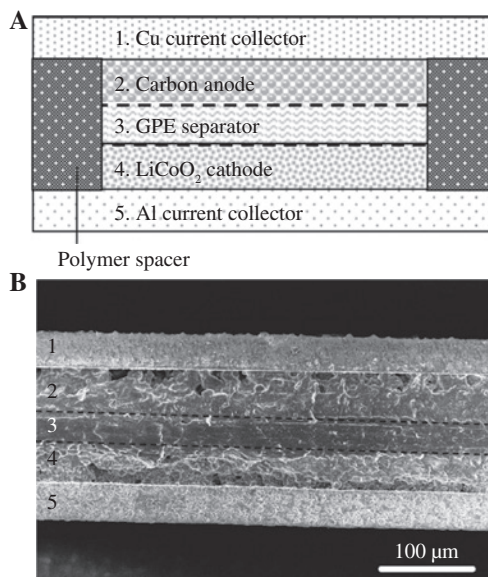


Figure 23: Cross-sectional view, (A) schematic, and (B) SEM micrograph of a lithium-ion micro-battery fabricated by LIFT. Reprinted from [44].

research has examined the effects of laser processing parameters on battery performance. In particular, the orientation and texture of electrodes, e.g. LiCoO_2 , produced in the LIFT process could have a significant effect on the electrochemical performance [113, 114]. The combination of printing of LMO electrodes by LIFT and subsequent fs-laser structuring was shown by Pröll et al. [11]. An array of 3D grid rectangular electrode structures were established, and an improvement in high rate capability was achieved. Rosenberg and Hintennach [115] proposed a LIFT approach using excimer laser, and they could demonstrate successfully the printing of lithium-sulfur-based electrodes. An up-scaling of this technology for HE cells with footprint areas up to $9 \times 18 \text{ cm}^2$ was proposed.

6.4 Electrolyte wetting

A main issue in cell production is the wetting of composite electrodes and separator materials with liquid electrolyte which is realized by time- and cost-consuming vacuum and storage processes at elevated temperatures [26, 45]. The liquid electrolyte has to be forced into micro- and nano-sized pores of the electrode and separator materials. Nevertheless, by applying current electrolyte filling processes, insufficient wetting of battery materials is one drawback resulting in a certain production failure rate, a lowered cell capacity, or a reduced battery lifetime. Laser structuring has been successfully applied for the formation of capillary microstructures in separators [21] and thick-film tape-cast electrodes resulting in an acceleration and homogeneity of electrolyte wetting. For thick-film composite electrodes an appropriate structure design delivers the most efficient capillary transport, and it could be shown that a huge impact on battery performance regarding battery lifetime and capacity retention at high charging and discharging currents could be achieved [13].

The capillary rise h of the electrolyte liquids along the laser-generated micro-capillary structures can in principle be described by the classical Washburn equation [13]:

$$\frac{dh}{dt} = \frac{r^2}{8\mu h} \left(\frac{2\sigma_l \cos\theta}{r} - \Delta\rho g h \right) \quad (4)$$

where h [m] is the height of capillary rise of the liquid within the capillary, t [s] is the capillary rise time, σ_l [kg/s²] and μ [kg/(ms)] are the surface tension and viscosity of the liquid, r [m] is the capillary radius, $\Delta\rho$ [kg/m³] is the difference in density between liquid and the gas-phase, g [m/s²] is the acceleration due to gravity, and θ [°] is the contact angle between the wall and the meniscus.

By neglecting the gravity and assuming that the capillary structure is filled at the beginning ($t=0$ s) up to a height of $h=h_0$, the integration of equation (4) delivers

$$h = h_0 + \sqrt{\frac{r\sigma_l \cos \theta}{2\mu}} \cdot t_h = h_0 + K \cdot t_h^{0.5} \quad (5)$$

where K [$\text{m/s}^{0.5}$] describes the penetration ability of the liquid, and t_h [s] the capillary rise time for achieving the height h [m].

The capillary rise of liquid electrolyte in laser-generated micro-channels in composite NMC electrodes could be described by equation (5) [13]. Recently, comparative studies of capillary rise in micro channels produced by embossing were performed (Figure 24A). It can be clearly seen that embossing leads to an inhomogeneity in material density, which in turn will have an impact on the porosity distribution. The edges of the generated channels were compressed which completely differs to the edges of the micro-channels produced by laser ablation (Figure 24B). Laser ablation provided open porosity along the generated sidewalls. The wetting behavior of capillary structures produced by these two methods is quite different (Figure 25A). For the laser-generated capillary structures a penetration

ability of 12 [equation (5)] could be reached, while for embossed channels only a value of two was obtained. After 20 s the embossed electrodes achieved a capillary rise of about 10 mm, while the laser-generated capillaries were filled with electrolyte up to 54 mm. Finally, the battery performances, the capacity as a function of cycle number, was investigated (Figure 25B). Cells assembled with embossed NMC electrodes rapidly dropped in capacity. After 100 cycles only 87% capacity retention was achieved, while for cells with laser-structured NMC electrodes the capacity retention is better than 99% (93% after 1000 cycles, not shown here). It is obvious that embossing, which could be easily performed during the conventional calendaring processing step in battery manufacturing, is not a suitable technology in order to replace laser structuring.

Laser-structured composite electrodes were developed for high-rate capability as well as for transforming regular electrode surfaces to superwicking for quick and efficient electrolyte impregnation [12, 116, 117]. It has been demonstrated that this process allows for the complete and rapid wetting of the electrode materials with liquid electrolyte [118]. Homogeneous wetting of electrode materials for LIBs is one of the basic requirements for proper

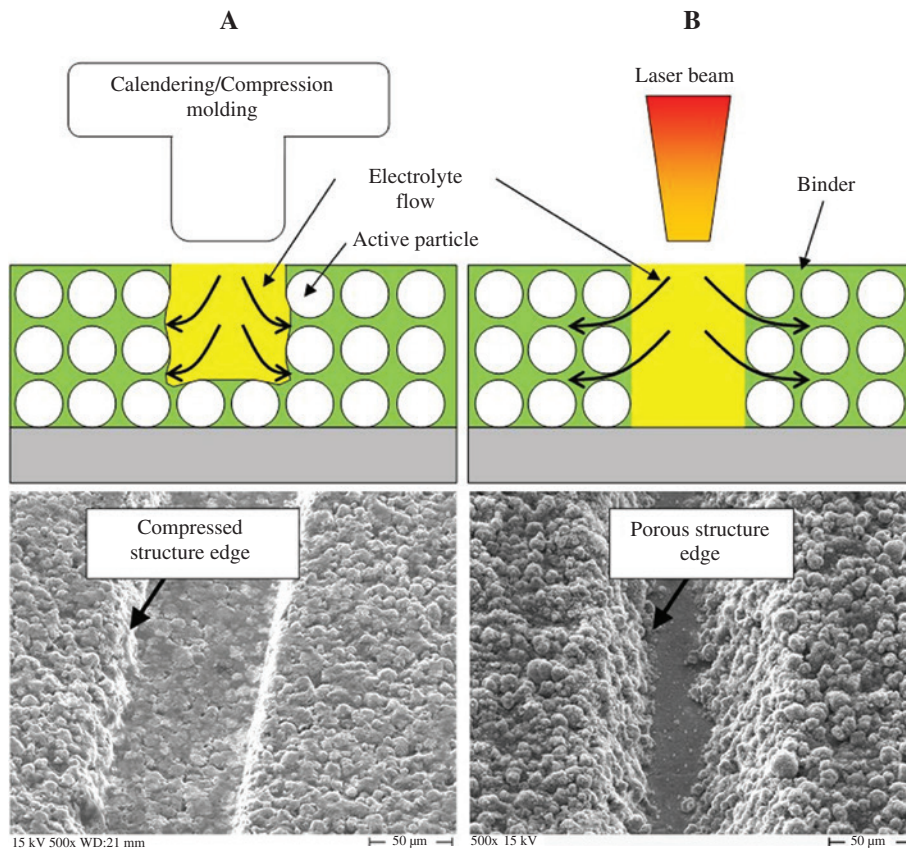


Figure 24: Capillary structures produced in NMC by embossing (A) in comparison to micro-channels generated by laser ablation (B).

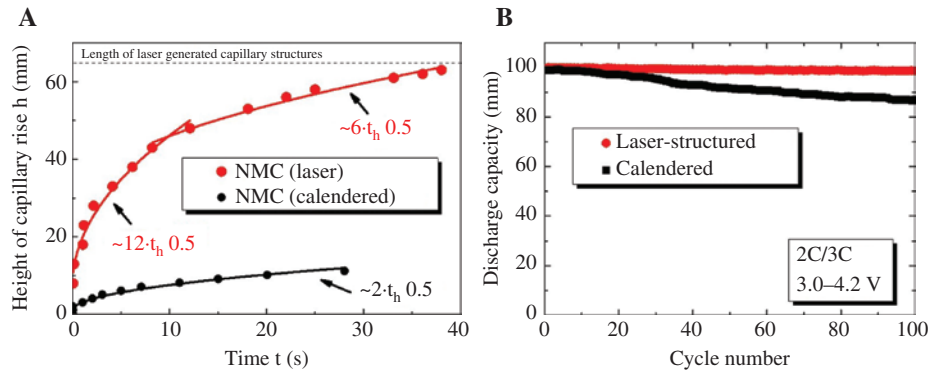


Figure 25: Comparison between laser structuring and structuring via embossing/calendering: (A) height of capillary rise as a function of time for structured NMC, and (B) discharge capacity as a function of cycle number for cells with laser-structured and embossed NMC.

cell operation especially under challenging conditions such as charging and discharging at high currents.

Proper electrolyte filling is still a challenging issue in industrial production of large-area LIB pouch cells where failure rates have to be minimized. Integration of laser processing technology into battery manufacturing will provide new impacts to process reliability, processing cost reduction, improved battery performance, and battery safety. Especially for HE batteries, wetting of the electrodes with liquid electrolyte is a critical issue. Large electrode sheets (e.g. 21×24 cm² [26]) are used, and in high-current cell, anodes and cathodes – separated by electrically insulating separator foils – are stacked until capacities of e.g. 40–60 Ah are reached. For this purpose, stacks of up to 100 individual layers are built up. After stacking which represents a technical challenge, this stack has to be filled with liquid electrolyte, such that the electrolyte penetrates the individual layers of the stack, and these layers are wetted completely and homogeneously. Due to the high vapor pressure of the liquid electrolyte, the filling process has to take place in a controlled and reliable manner. In the manufacture of cells on a large technical scale, it is presently tried to accomplish homogeneous electrolyte wetting by expensive and time-consuming vacuum and storage processes at elevated temperatures [26]. However, it has to be assumed that in spite of this high technical expenditure, a certain production failure rate is caused by insufficient electrode wetting in the manufactured cell. Insufficient electrolyte wetting would lead to dry areas in the cell, which are not contributing to electrochemical reactions leading to a decrease of the overall cell capacity. Those hot spots are starting points for cell degradation and cell failure under challenging cycling conditions. This is the only reason why the massive technical expenditure of the process steps of electrolyte filling and storage at elevated temperatures, which require investments of millions in commercial cell manufacture lines, are

accepted. The laser-based structuring technology will accelerate the wetting process and will lead to a homogenized electrolyte wetting. It is assumed that due to laser processing the warm aging process of several days (72–96 h) can be avoided, which will lead to a reduction of energy and power consumption. Additional costs for vacuum, storage room, and logistic can be avoided. Finally, the 3D battery concept can reduce the cell manufacturing costs by 20%. These values were taken from Wood et al. [26] with estimated cell costs of 272 \$/kWh on base of a 52 Ah pouch cell (NMC). The thick-film concept will lead to an increase of 20–30% in specific cell capacity (Figure 6). Material costs and production costs can be further reduced due to less inactive material and less processing steps, respectively. Under the assumption that an overall cost reduction of “only” 20% can be achieved, the cell cost would drop by a value of 50 €/kWh. For an electrical vehicle with 55 kWh (100 cells), a benefit of about 2800 € could be obtained (28 € per cell). It is obvious that the laser process will have also an impact on the battery manufacturing cost. A rough estimation of the laser throughput taking into account the conventional electrode coating speed (30 m/min) leads to the assumption that a single production line will consist of about three laser machines. Over a period of 5 years electrodes for approximately 5 Mio cells can be laser structured for a budget of about 5 Mio € including the laser investment costs of about 1.5 Mio €. Under these assumptions, the laser process will lead to an increase in manufacturing cost of about 1 €/cell which is significantly smaller than the above mentioned benefit of about 28 €/cell. Nevertheless, it should be pointed out that the laser machines, their maintenance, and the required optical devices, e.g. polygon scanner, are currently cutting edge technology, and a fully proven concept and machine design is still required to be developed.

The above mentioned assumptions regarding processing costs need to be critically reviewed regarding the

electrode footprint area. For a large footprint area, the time-dependent electrolyte wetting might need a certain time, even with support by capillary structures. For the boundary condition $dh/dt (h = h_{\max}) = 0$ a maximum height of capillary rise of about 20 cm could be calculated from equation (4) for a wetting arrangement versus gravity [13] which is in good agreement with typical dimensions of a 40 Ah cell. But it is also clear from Figure 25A that wetting of large footprint areas could take several minutes. Finally, an experimental evaluation for large footprint areas and large number of electrode stacks is necessary in order to prove the reduction in processing costs.

In a first approach, the impact of laser-generated capillary structures was evaluated by producing pouch cells with footprint areas of 25 cm² with structured and unstructured NMC cathodes [13]. While lithium-ion pouch cells with unstructured NMC electrodes spontaneously fail within a cycle number range of 1000–1500, lithium-ion cells with laser-structured NMC electrodes indicated a stable cycling behavior up to 3000 cycles resulting in specific charge and discharge capacities of approximately 105 mAh/g (Figure 26). It could be shown that high coulomb efficiency can be reached even during long-term cycling. After 500 cycles the capacity retention of the cells with unstructured NMC electrode is 89%, while the capacity retention for cells with laser-structured NMC electrode is 94%. After 1000 cycles the capacity retention for cells with unstructured NMC electrode counts 85%. Concerning lithium-ion cells with laser-structured NMC electrode as well as after 1000 cycles, the capacity retention drops to 89%. A critical capacity value for lithium-ion cells is the 80% limit of the initial capacity. When reaching a capacity

retention of 80%, the so-called “cell lifetime” is achieved. Lithium-ion cells with laser-structured NMC cathodes exhibited the longest lifetime with 2290 cycles. The 80% limit was reached for lithium-ion cells with unstructured NMC cathodes at 1199 cycles. Cells with unstructured NMC electrodes show a spontaneous failure after 1600 cycles, while cells with laser-structured NMC electrodes show only a slight decrease in capacity with increasing cycle number leading to a capacity of about 60% of the initial capacity after 10,000 cycles (Figure 26).

Regarding processing cost in battery manufacturing, the use of cost-efficient ns-laser radiation for the structuring process would be preferred. Therefore, the formation of capillary structures using ns-laser ablation as well as ultrafast laser processing was investigated. For ns-laser radiation (wavelength 1064 nm, pulse length 200 ns) the laser beam energy is absorbed at the material surface, and due to heat conduction the temperature of the surrounding composite material increases. The binder material for tape cast electrodes (~5 wt%) is polyvinylidene difluoride (PVDF), which has a low decomposition temperature in the range of 250–350°C [119]. Therefore, the PVDF binder matrix spontaneously evaporates, and active particles are removed from the laser beam interaction zone, which was demonstrated for the patterning of NMC electrodes (Figure 24B) [13]. A similar ablation process for metal/polymer composite materials has been described by Slocombe and Li [120]. Nanosecond laser ablation is not appropriate for each type of electrode material. For example, ns-laser structuring of LFP electrodes leads to melt formation and to an undesired modification of the active material, very similar to the already discussed phase changes which occur during laser cutting of LFP (see Section 4). The thermal impact of laser processing can be significantly reduced by using ultrafast laser ablation. Furthermore, the ablation efficiency of LFP increases by a factor of 3 by using femto- or picosecond laser ablation in comparison to ns-laser ablation [117]. For battery production costs it is important to reduce the amount of ablated material which in turn means that small-capillary widths and high aspect ratios are preferred. By using ultrafast laser ablation, it could be shown that the aspect ratio could be significantly increased and that the loss of active material can be reduced from 20% down to values below 5%.

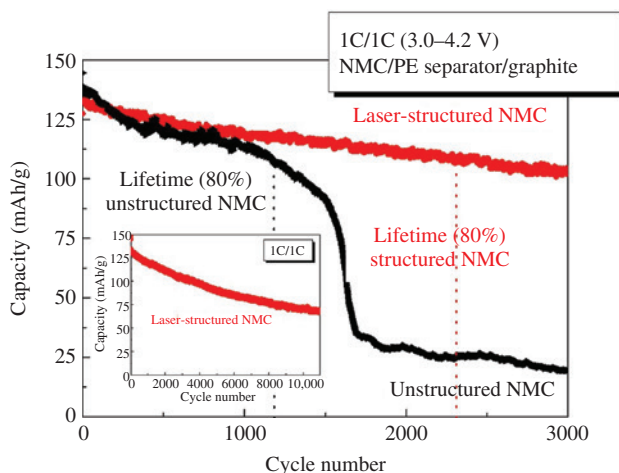


Figure 26: Specific discharge capacities of pouch cells with unstructured and structured NMC cathodes for cycle numbers up to $n = 3000$ cycles and 10,000 cycles (inset diagram), respectively.

7 Future perspectives

To get chemical change information in battery materials on submicron and micrometer scales, there can be several

technologies applied *ex situ* and *post-mortem*. Such very well-established technologies are, e.g. X-ray photoelectron spectroscopy (XPS), Auger electron spectroscopy (AES), EDX, or TOF-SIMS. Besides the problem to have a low lithium sensitivity for technologies such as XPS or AES, all of these technologies suffer in general from a large measuring time, measuring under vacuum conditions, and a limitation in information depth and measuring area. For a chemical mapping of a complete electrode down to the current collector, laser-induced breakdown spectroscopy (LIBS) seems to be an appropriate analytical technique, which is quite sensitive to lithium detection. There are only a few groups that are using this technology for investigating battery materials [60, 103, 121–125]. Hou et al. [122] realized a 3D multi-elemental mapping of solid electrolyte material in a 3D space of $1.11 \times 1.11 \times 0.035 \text{ mm}^3$ with $74 \text{ }\mu\text{m}$ lateral resolution. In a rather new approach large areal NMC electrodes ($5 \times 5 \text{ cm}^2$) with a thickness of $100 \text{ }\mu\text{m}$, or even thicker, were entirely investigated by LIBS with a lateral resolution of $100 \text{ }\mu\text{m}$ [124]. It is a rather new approach to apply LIBS for a comprehensive chemical characterization for complete large areal and thick-film electrodes down to the current collector in order to investigate chemical degradation mechanisms and the impact of 3D electrode architectures on lithium distribution [60, 103, 123, 124, 126]. It could be shown so far that 3D electrode structures can provide new lithium-insertion paths, which enhance the capability of the electrode material to accept high charging/discharging currents (Figure 20). LIBS can be used for local chemical analysis such as element depth profiling and element mapping of cycled electrodes.

Finally, new scientific findings regarding degradation mechanisms due to electrochemical aging of advanced electrode materials with different cell architectures (structured, unstructured) can be explored. In summary, the mechanisms associated with the performance evaluation of 3D structure micro-battery and the structure and chemical evolution on nanometer and micrometer scale are an important leading basic subject for the development of HE/high-power density batteries.

Figure 27 shows an example for a lithium mapping of an electrochemically cycled unstructured electrode. LIBS was performed for an area of $5 \times 5 \text{ cm}^2$, which corresponds to the footprint area of the electrode. The electrode was used as NMC cathode in a 45 mAh pouch cell with a polyolefin separator and graphite as counter electrode. Before assembly, a periodic through-hole-pattern was generated by fs-laser radiation into the separator material in order to reinforce the battery degradation process. A significant cell degradation was achieved after 1000 cycles. After the cell capacity dropped down to 10 mAh , the cell was disassembled. Figure 27A provides 3D information of the lithium concentration in different layers. The 2D mapping (Figure 27B) shows the lithium concentration along the electrode surface which is varied, and obviously two spots with a significant lithium increase could be detected. These spots are related to lithium plating, which in turn can induce an electrical shortcut in the battery and a drop in capacity. It was shown that chemical degradation can be illustrated for a complete pouch cell by using LIBS. The impact of laser-structured electrodes on the lithium distribution was recently investigated [60, 103, 124].

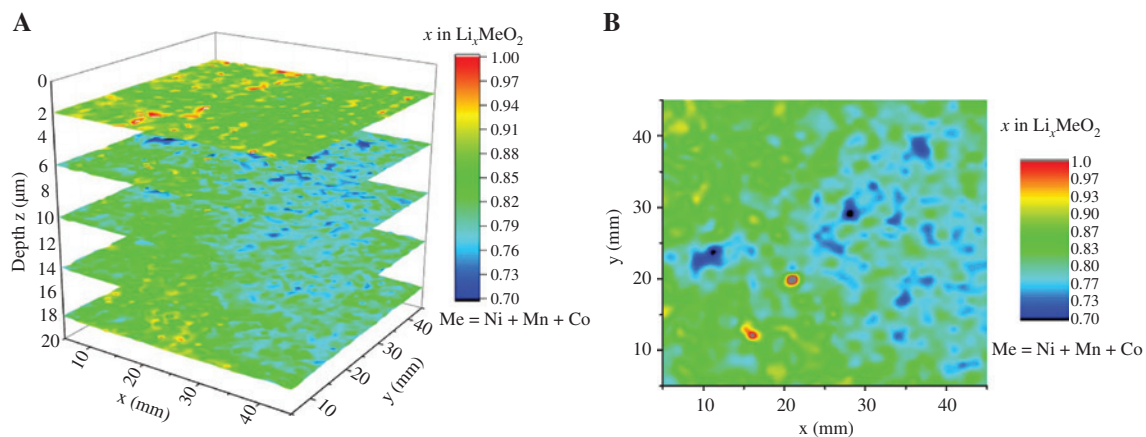


Figure 27: LIBS lithium elemental mapping of an electrochemically cycled and degraded NMC pouch cell electrode ($5 \times 5 \text{ cm}^2$). The amount of x of lithium in $\text{Li}_x\text{Ni}_{1/3}\text{Mn}_{1/3}\text{Co}_{1/3}\text{O}_2$ is illustrated. (A) 3D layer-by-layer contour map of lithium concentration, and (B) 2D mapping of lithium concentration (second layer). The depth per pulse is $4 \text{ }\mu\text{m}$.

8 Conclusions

Several laser processes and their impact on battery performance were presented. These technologies show different types of readiness level regarding up-scaling and a possible integration in state-of-the-art battery production lines. For laser cutting of electrodes a high degree of process readiness level is achieved, and commercial ns-laser cutter systems adapted to battery manufacturing are available and can be introduced in cell manufacturing. Nevertheless, laser cutting will be further developed regarding next generation of batteries using the thick-film concept. Ultrafast laser cutting of electrodes offers improved cut edge qualities, less debris formation, and an improved ablation efficiency, which will be essential for a new electrode cutter generation.

The processing speed of laser drying of electrodes seems to be a main drawback. In general, fast drying of electrodes will raise problems of crack formation and mechanical stability of the electrodes. This will get even worse by the required transfer of this technology to thick-film electrode materials ($>100\ \mu\text{m}$). In ongoing research, an up-scaling of this technology and a precise adjustment of process parameters will be necessary and is meaningful regarding an important contribution for saving of energy in battery production lines.

Laser structuring of composite electrodes is one of the most promising approaches regarding battery performance improvement by the 3D battery concept and an increase of battery safety and production reliability. A homogenous and rapid electrode wetting with liquid electrolyte has several advantages, such as a significant reduction of production costs, an increased battery lifetime, and an easy transfer of this technology to HE and high-power batteries using the thick-film concept. The increased lifetime will be further reinforced by providing liquid electrolyte reservoirs in laser-generated artificial porosity. Due to long lifetimes and a flexible use of those batteries in stand-alone energy storage devices or electrical vehicles, second-life applications will become possible leading to an environmental sustainable use.

For ongoing research and development, laser technologies need to be adapted to new materials, processing speeds, and footprint areas provided in state-of-the-art and next generation battery production lines. Furthermore, a processing match or selection of laser technologies to different cell designs, such as pouch cells, prismatic cells, or cylindrical cells, will be necessary.

Acknowledgments: We acknowledge support by Deutsche Forschungsgemeinschaft and Open Access Publishing

Fund of Karlsruhe Institute of Technology. This work received funding from the European Union's Horizon 2020 research and innovation programme under the Marie Skłodowska-Curie grant agreement no. 644971. Finally, the support for laser materials processing by the Karlsruhe Nano Micro Facility (KNMF, <http://www.knmf.kit.edu/>) a Helmholtz research infrastructure at the Karlsruhe Institute of Technology (KIT) is gratefully acknowledged.

References

- [1] Goodenough JB, Kim Y. Challenges for rechargeable Li batteries. *Chem Mater* 2010;22:587–603.
- [2] Scrosati B, Garche J. Lithium batteries: status, prospects and future. *J Power Sources* 2010;195:2419–30.
- [3] Amatucci G, Du Pasquier A, Blyr A, Zheng T, Tarascon JM. The elevated temperature performance of the $\text{LiMn}_2\text{O}_4/\text{C}$ system: failure and solutions. *Electrochim Acta* 1999;45:255–71.
- [4] Andre D, Kim S-J, Lamp P, et al. Future generations of cathode materials: an automotive industry perspective. *J Mater Chem A* 2015;3:6709–32.
- [5] Sakti, A. Quantification of performance and cost trajectory of Li-ion battery designs for personal vehicle electrification in the near future. Carnegie Mellon University, ProQuest Dissertations Publishing, page 118, 2014.
- [6] Kirchhoff M. Laser applications in battery production – from cutting foils to welding the case. In: 2013 3rd International Electric Drives Production Conference (EDPC) 1–3, 2013.
- [7] De Bono P, Blackburn J. Laser welding of copper and aluminium battery interconnections. *Proc SPIE* 2015;9657:96570M.
- [8] Schmidt PA, Schmitz P, Zaeh MF. Laser beam welding of electrical contacts for the application in stationary energy storage devices. *J Laser Appl* 2016;28:022423.
- [9] Brand MJ, Schmidt PA, Zaeh MF, Jossen A. Welding techniques for battery cells and resulting electrical contact resistances. *J Energy Storage* 2015;1:7–14.
- [10] Kohler R, Pröll J, Bruns M, Ulrich S, Seifert HJ, Pflöging W. Conical surface structures on model thin-film electrodes and tape-cast electrode materials for lithium-ion batteries. *Appl Phys A* 2013;112:77–85.
- [11] Pröll J, Kim H, Piqué A, Seifert HJ, Pflöging W. Laser-printing and femtosecond-laser structuring of LiMn_2O_4 composite cathodes for Li-ion microbatteries. *J Power Sources* 2014;255:116–24.
- [12] Kim H, Pröll J, Kohler R, Pflöging W, Pique A. Laser-printed and processed LiCoO_2 cathode thick films for Li-Ion microbatteries. *J Laser Micro Nanoen* 2012;7:320–5.
- [13] Pflöging W, Pröll J. A new approach for rapid electrolyte wetting in tape cast electrodes for lithium-ion batteries. *J Mater Chem A* 2014;2:14918–26.
- [14] Kim JS, Pflöging W, Kohler R, et al. Three-dimensional silicon/carbon core-shell electrode as an anode material for lithium-ion batteries. *J Power Sources* 2015;279:13–20.
- [15] Tang X-X, Liu W, Ye B-Y, Tang Y. Preparation of current collector with blind holes and enhanced cycle performance of silicon-based anode. *Trans Nonferrous Met Soc China* 2013;23:1723–7.

- [16] Long JW, Dunn B, Rolison DR, White HS. Three-dimensional battery architectures. *Chem Rev* 2004;104:4463–92.
- [17] Notten PHL, Roozeboom F, Niessen RAH, Baggetto L. 3-D integrated all-solid-state rechargeable batteries. *Adv Mater* 2007;19:4564–7.
- [18] Oudenhoven JFM, Baggetto L, Notten PHL. All-solid-state lithium-ion microbatteries: a review of various three-dimensional concepts. *Adv Energy Mater* 2011;1:10–33.
- [19] Ferrari S, Loveridge M, Beattie SD, Jahn M, Dashwood RJ, Bhagat R. Latest advances in the manufacturing of 3D rechargeable lithium microbatteries. *J Power Sources* 2015;286:25–46.
- [20] Kohler R, Besser H, Hagen M, et al. Laser micro-structuring of magnetron-sputtered SnO_x thin films as anode material for lithium ion batteries. *Microsyst Technol* 2011;17:225–32.
- [21] Pröll J, Schmitz B, Niemöeller A, et al. Femtosecond laser patterning of lithium-ion battery separator materials: impact on liquid electrolyte wetting and cell performance. *Proc SPIE* 2015;9351:1F1–7.
- [22] Liu HK, Wang GX, Guo Z, Wang J, Konstantinov K. Nanomaterials for lithium-ion rechargeable batteries. *J Nanosci Nanotechnol* 2006;6:1–15.
- [23] Daniel C, Mohanty D, Li J, Wood DL. Cathode materials review. *AIP Conference Proceedings* 2014;1597:26–43.
- [24] Nitta N, Wu FX, Lee JT, Yushin G. Li-ion battery materials: present and future. *Mater Today* 2015;18:252–64.
- [25] Thackeray MM, Wolverton C, Isaacs ED. Electrical energy storage for transportation – approaching the limits of, and going beyond, lithium-ion batteries. *Energy Environ Sci* 2012;5:7854–63.
- [26] Wood DL, Li JL, Daniel C. Prospects for reducing the processing cost of lithium ion batteries. *J Power Sources* 2015;275:275234–42.
- [27] Koller S, Kren H, Schmuck M, et al. Next-generation materials for electrochemical energy storage – silicon and magnesium. *AIP Conference Proceedings* 2016;1765:020007.
- [28] Roberts M, Johns P, Owen J, et al. 3D lithium ion batteries-from fundamentals to fabrication. *J Mater Chem* 2011;21:9876–90.
- [29] Patil A, Patil V, Shin DW, Choi JW, Paik DS, Yoon SJ. Issue and challenges facing rechargeable thin film lithium batteries. *Mater Res Bull* 2008;43:1913–42.
- [30] Kanehori K, Matsumoto K, Miyauchi K, Kudo T. Thin-film solid electrolyte and its application to secondary lithium cell. *Solid State Ion* 1983;9–10:1445–8.
- [31] Schneider CW, Lippert T. Laser ablation and thin film deposition. In: Schaaf P., ed. *Laser processing of materials*, Berlin, Springer, 2010, 89–112.
- [32] Willmott PR, Huber JR. Pulsed laser vaporization and deposition. *Rev Mod Phys* 2000;72:315–28.
- [33] Montenegro MJ, Lippert T. Films for electrochemical applications. In: Eason R., ed. *Pulsed laser deposition of thin films: applications-led growth of functional materials*, John Wiley & Son Inc., Hoboken, New Jersey, 2007, 563–584.
- [34] Beck G, Poepke H, Luerssen B, Janek J. Microstructure of platinum films on YSZ prepared by pulsed laser deposition. *J Cryst Growth* 2011;322:95–102.
- [35] Huber A-K, Falk M, Rohnke M, et al. In situ study of electrochemical activation and surface segregation of the SOFC electrode material $\text{La}_{0.75}\text{Sr}_{0.25}\text{Cr}_{0.5}\text{Mn}_{0.5}\text{O}_{3+\delta}$. *Phys Chem Chem Phys* 2012;14:751–8.
- [36] Jiang LZ, Zhou MF, Liu XN, Qin QZ. CeO_2 thin film as a lithium-ion-storage material fabricated by pulsed laser deposition. *Acta Phys-Chim Sin* 1999;15:752–6.
- [37] Zhao SL, Fu ZW, Qin QZ. A solid-state electrolyte lithium phosphorus oxynitride film prepared by pulsed laser deposition. *Thin Solid Films* 2002;415:108–13.
- [38] Zhao SL, Qin QZ. Li-V-Si-O thin film electrolyte for all-solid-state Li-ion battery. *J Power Sources* 2003;122:174–80.
- [39] Inaba M, Doi T, Iriyama Y, Abe T, Ogumi Z. Electrochemical STM observation of LiMn_2O_4 thin films prepared by pulsed laser deposition. *J Power Sources* 1999;81:554–7.
- [40] Sun JP, Tang K, Yu XQ, Li H, Huang XJ. Needle-like LiFePO_4 thin films prepared by an off-axis pulsed laser deposition technique. *Thin Solid Films* 2009;517:2618–22.
- [41] Rahn J, Hüger E, Dörrer L, Ruprecht B, Heitjans P, Schmidt H. Self-diffusion of lithium in amorphous lithium niobate layers. *Z Phys Chem* 2012;226:439–48.
- [42] Rahn J, Hüger E, Dörrer E, Ruprecht B, Heitjans P, Schmidt H. A SIMS study on Li diffusion in single crystalline and amorphous LiNbO_3 . *Defect Diffus Mater* 2012;323–325:69–74.
- [43] Li J, Daniel C, Wood D. Materials processing for lithium-ion batteries. *J Power Sources* 2011;196:2452–60.
- [44] Kim H, Auyeung RCY, Piqué A. Laser-printed thick-film electrodes for solid-state rechargeable Li-ion microbatteries. *J Power Sources* 2007;165:413–9.
- [45] Wollersheim O, Pflöging W. Optimierte Fertigungslogistik Neuartige Elektrolytbefüllung für Lithium-Ionen-Zellen. *ATZelektronik* 2012;7:52–5.
- [46] Luetke M, Franke V, Techel A, et al. A comparative study on cutting electrodes for batteries with lasers. *Phys Procedia* 2011;12:286–91.
- [47] Demir AG, Previtali B. Remote cutting of Li-ion battery electrodes with infrared and green ns-pulsed fibre lasers. *Int J Adv Manuf Tech* 2014;75:1557–68.
- [48] Lutey AHA, Fortunato A, Carmignato S, Ascari A, Liverani E, Guerrini G. Quality and productivity considerations for laser cutting of LiFePO_4 and LiNiMnCoO_2 battery electrodes. *Proc CIRP* 2016;42:433–8.
- [49] Schmieder B. Laser cutting of graphite anodes for automotive lithium-ion secondary batteries: investigations in the edge geometry and heat affected zone. *Proc SPIE* 2012;8244: 0R1–7.
- [50] Kronthaler MR, Schloegl F, Kurfer J, Wiedenmann R, Zaeh MF, Reinhart G. Laser cutting in the production of lithium ion cells. *Phys Procedia* 2012;39:213–24.
- [51] Schmieder B. Analytical model of the laser ablation mechanism of lithium-ion battery coatings. *Proc SPIE* 2015;9351:1C1–13.
- [52] Kurfer J, Westermeier M, Tammer C, Reinhart G. Production of large-area lithium-ion cells – preconditioning, cell stacking and quality assurance. *CIRP Ann Manuf Tech* 2012;61:1–4.
- [53] Gotcu P, Pflöging W, Smyrek P, Seifert HJ. Thermal behaviour of Li_xMeO_2 (Me = Co or Ni + Mn + Co) cathode materials. *Phys Chem Chem Phys* 2017;19:11920–30.
- [54] Chen Z, Wang J, Chao D, et al. Hierarchical porous $\text{LiNi}(1/3)\text{Co}(1/3)\text{Mn}(1/3)\text{O}(2)$ nano-/micro spherical cathode material: minimized cation mixing and improved $\text{Li}(+)$ mobility for enhanced electrochemical performance. *Sci Rep* 2016;6:25771.
- [55] Pflöging W, Przybylski M, Bruckner HJ. Excimer laser material processing – state of the art and new approaches in microsystem technology. *Proc SPIE* 2006;6107:0G1–15.

- [56] Eaton SM, Zhang H, Herman PR, et al. Heat accumulation effects in femtosecond laser-written waveguides with variable repetition rate. *Opt Express* 2005;13:4708–16.
- [57] Gattass RR, Mazur E. Femtosecond laser micromachining in transparent materials. *Nat Photonics* 2008;2:219–25.
- [58] Sugioka K. Ultrafast laser processing of glass down to the nano-scale. In: Miotello A., Ossi P., eds. *Laser-Surface Interactions for New Materials Production*. Springer Series in Materials Science, Berlin, Heidelberg, Springer, 2010;130:279–93.
- [59] Sugioka K, Hanada Y, Midorikawa K. Three-dimensional femtosecond laser micromachining of photosensitive glass for biomicrochips. *Laser Photon Rev* 2010;4:386–400.
- [60] Pflöging W, Zheng Y, Mangang M, Bruns M, Smyrek P. Laser processes and analytics for high power 3D battery materials. *Proc SPIE* 2016;9740: 131–9.
- [61] Lee D, Patwa R, Herfurth H, Mazumder J. High speed remote laser cutting of electrodes for lithium-ion batteries: anode. *J Power Sources* 2013;240:368–80.
- [62] Lutey AHA, Fortunato A, Ascari A, Carmignato S, Leone C. Laser cutting of lithium iron phosphate battery electrodes: characterization of process efficiency and quality. *Opt Laser Technol* 2015;65:164–74.
- [63] Lutey AHA, Fiorini M, Fortunato A, Ascari A. Chemical and microstructural transformations in lithium iron phosphate battery electrodes following pulsed laser exposure. *Appl Surface Sci* 2014;322:85–94.
- [64] Lutey AHA, Fiorini M, Fortunato A, Carmignato S. Lithium iron phosphate battery electrode integrity following high speed pulsed laser cutting. *Appl Phys A* 2015;119:431–5.
- [65] Hwang KH, Lee SH, Joo SK. Fabrication and characterization of an Li-Mn-O thin-film cathode for rechargeable lithium micro-batteries. *J Power Sources* 1995;54:224–7.
- [66] Kim KW, Lee S-W, Han K-S, Chung HJ, Woo SI. Characterization of Al-doped spinel LiMn_2O_4 thin film cathode electrodes prepared by liquid source misted chemical deposition (LSMCD) technique. *Electrochim Acta* 2003;48:4223–31.
- [67] Wu XM, Li XH, Wang Z, Xiao ZB, Liu J, Yan WB. Characterization of solution-derived LiMn_2O_4 thin films heat-treated by rapid thermal annealing. *Mater Chem Phys* 2004;83:78–81.
- [68] Wu XY, Huang GH, Liu L, Li JB. An interval nonlinear program for the planning of waste management systems with economies-of-scale effects – a case study for the region of Hamilton, Ontario, Canada. *Eur J Oper Res* 2006;171:349–72.
- [69] Chiu K-F, Hsiao HH, Chen GS, Liu HL, Her JL, Lin HC. Structural evolution and stability of RF sputter deposited $\text{Li}_x\text{Mn}_{2-y}\text{O}_4$ thin film cathodes. *J Electrochem Soc* 2004;151:A452–5.
- [70] Ryu S-G, Gruber I, Grigoropoulos CP, Poulidakos D, Moon S-J. Large area crystallization of amorphous Si with overlapping high repetition rate laser pulses. *Thin Solid Films* 2012;520:6724–9.
- [71] Ye R, Yamani Y, Ohta K, Baba M. Laser modification and characterization of LiMn_2O_4 cathodes for thin film lithium-ion battery. *ECS Trans* 2014;59:79–84.
- [72] Kohler R, Smyrek P, Ulrich S, Bruns M, Trouillet V, Pflöging W. Patterning and annealing of nanocrystalline LiCoO_2 thin films. *J Optoelectron Adv M* 2010;12:547–52.
- [73] Pröll J, Kohler R, Torge M, et al. Laser microstructuring and annealing processes for lithium manganese oxide cathodes. *Appl Surface Sci* 2011;257:9968–76.
- [74] Pröll J, Weidler PG, Kohler R, et al. Comparative studies of laser annealing technique and furnace annealing by X-ray diffraction and Raman analysis of lithium manganese oxide thin films for lithium-ion batteries. *Thin Solid Films* 2013;531:160–71.
- [75] Pröll J, Kohler R, Mangang A, et al. Diode laser heat treatment of lithium manganese oxide films. *Appl Surface Sci* 2012;258:5146–52.
- [76] Julien CM, Massot M. Lattice vibrations of materials for lithium rechargeable batteries III. Lithium manganese oxides. *Mater Sci Eng B* 2003;100:69–78.
- [77] Park SH, Sato Y, Kim J-K, Lee Y-S. Powder property and electrochemical characterization of Li_2MnO_3 material. *Mater Chem Phys* 2007;102:225–30.
- [78] Julien CM, Massot M. Lattice vibrations of materials for lithium rechargeable batteries I. Lithium manganese oxide spinel. *Mater Sci Eng B* 2003;97:217–30.
- [79] Günther T, Billot N, Schuster J, Schnell J, Spingler FB, Gasteiger HA. The manufacturing of electrodes: key process for the future success of lithium-ion batteries. *Adv Mat Res* 2016;1140: 304–11.
- [80] Li J, Daniel C, An SJ, Wood D. Evaluation residual moisture in lithium-ion battery electrodes and its effect on electrode performance. *MRS Adv* 2016;1:1029–35.
- [81] Vedder C, Hawelka D, Wolter M, Leiva D, Stollenwerk J, Wissenbach K. Laser-based drying of battery electrode layers. In: *The 35th International Congress on Applications of Lasers & Electro-Optics (ICALEO) N501-501–N501-506*, 2016.
- [82] Hawelka D. Battery production: laser light instead of oven-drying and vacuum technology. *Laser Tech J* 2015;12:16.
- [83] Zadin V, Kasemagi H, Aabloo A, Brandell D. Modeling electrode material utilization in the trench model 3D-microbattery by finite element analysis. *J Power Sources* 2010;195:6218–24.
- [84] Baggetto L, Niessen RAH, Roozeboom F, Notten PHL. High energy density all-solid-state batteries: a challenging concept towards 3D integration. *Adv Funct Mater* 2008;18:1057–66.
- [85] Lim DG, Chung DW, Kohler R, et al. Designing 3D conical-shaped lithium-ion microelectrodes. *J Electrochem Soc* 2014;161:A302–7.
- [86] Pikul JH, Zhang HG, Cho J, Braun PV, King WP. High-power lithium ion microbatteries from interdigitated three-dimensional bicontinuous nanoporous electrodes. *Nat Commun* 2013;4:1–5. Article No. 1732.
- [87] Zhang HG, Yu XD, Braun PV. Three-dimensional bicontinuous ultrafast-charge and -discharge bulk battery electrodes. *Nat Nanotechnol* 2011;6:277–81.
- [88] Xie J, Oudenhoven JFM, Li DJ, Chen CG, Eichel RA, Notten PHL. High power and high capacity 3D-structured TiO_2 electrodes for lithium-ion microbatteries. *J Electrochem Soc* 2016;163:A2385–9.
- [89] Hudaya C, Halim M, Proll J, et al. A polymerized C-60 coating enhancing interfacial stability at three-dimensional LiCoO_2 in high-potential regime. *J Power Sources* 2015;298:1–7.
- [90] Park JH, Kohler R, Pflöging W, Choi WC, Seifert HJ, Lee JK. Electrochemical behavior of a laser microstructured fluorine doped tin oxide anode layer with a plasma pretreatment for 3D battery systems. *Rsc Adv* 2014;4:4247–52.
- [91] Oh K-Y, Siegel JB, Secondo L, et al. Rate dependence of swelling in lithium-ion cells. *J Power Sources* 2014;267:197–202.

- [92] Su X, Wu QL, Li JC, et al. Silicon-based nanomaterials for lithium-ion batteries: a review. *Adv Energy Mater* 2014;4:1–23. Article No. 1300882.
- [93] Chen D, Indris S, Schulz M, Gamer B, Mönig R. In situ scanning electron microscopy on lithium-ion battery electrodes using an ionic liquid. *J Power Sources* 2011;196:6382–7.
- [94] Cho GB, Kim JK, Lee SH, et al. Facile fabrication of patterned Si film electrodes containing trench-structured Cu current collectors for thin-film batteries. *Electrochim Acta* 2017;224:649–59.
- [95] Han PX, Han XQ, Yao JH, Liu ZH, Cao XY, Cui GL. Flexible graphite film with laser drilling pores as novel integrated anode free of metal current collector for sodium ion battery. *Electrochem Commun* 2015;61:84–8.
- [96] Zhang N, Zheng Y, Trifonova A, Pflęging W. Laser structured Cu Foil for high-performance lithium-ion battery anodes. *J Appl Electrochemistry* 2017;47:829–37.
- [97] Zheng Y, Pröll J, Kunze T, et al. Laser direct interference patterning and ultrafast laser-induced micro/nano structuring of current collectors for lithium-ion batteries. *Proc SPIE* 2016;9740:1B1–7.
- [98] Ketterer B, Vasilchina H, Seemann K, et al. Development of high power density cathode materials for Li-ion batteries. *Int J Mater Res* 2008;99:1171–6.
- [99] Singh M, Kaiser J, Hahn H. Thick electrodes for high energy lithium ion batteries. *J Electrochem Soc* 2015;162:A1196–201.
- [100] Smyrek P, Pröll J, Rakebrandt JH, Seifert HJ, Pflęging W. Manufacturing of advanced Li(NiMnCo)O₂ electrodes for lithium-ion batteries. *Proc SPIE* 2015;9351:1D1–8.
- [101] Mottay E, Liu XB, Zhang HB, Mazur E, Sanatinia R, Pflęging W. Industrial applications of ultrafast laser processing. *MRS Bull* 2016;41:984–92.
- [102] Mangang M, Seifert HJ, Pflęging W. Influence of laser pulse duration on the electrochemical performance of laser structured LiFePO₄ composite electrodes. *J Power Sources* 2016;304:24–32.
- [103] Smyrek P, Pröll J, Seifert HJ, Pflęging W. Laser-induced breakdown spectroscopy of laser-structured Li(NiMnCo)O₂ electrodes for lithium-ion batteries. *J Electrochem Soc* 2016;163:A19–26.
- [104] Pröll J, Kohler R, Torge M, et al. Laser adjusted three-dimensional Li-Mn-O cathode architectures for secondary lithium-ion cells. *Proc SPIE* 2012;8244:0S1–10.
- [105] Pröll J, Kohler R, Bruns M, et al. Thin film passivation of laser generated 3D micro patterns in lithium manganese oxide cathodes. *Proc SPIE* 2013;8608:071–10.
- [106] Kohler R, Bruns M, Smyrek P, Ulrich S, Przybylski M, Pflęging W. Laser annealing of textured thin film cathode material for lithium ion batteries. *Proc SPIE* 2010;7585:0Q1–0Q11.
- [107] Kohler R, Pröll J, Ulrich S, et al. Laser-assisted structuring and modification of LiCoO₂ thin films. *Proc SPIE* 2009;7202:071–11.
- [108] Pröll J, Kohler R, Adelhelm C, et al. Laser modification and characterization of Li-Mn-O thin film cathodes for lithium-ion batteries. *Proc SPIE* 2011;7921:0Q1–14.
- [109] Pröll J, Kohler R, Mangang A, Ulrich S, Ziebert C, Pflęging W. 3D structures in battery materials. *J Laser Micro Nanoen* 2012;7:97–104.
- [110] Arnold CB, Kim H, Pique A. Laser direct write of planar alkaline microbatteries. *Appl Phys A* 2004;79:417–20.
- [111] Wartena R, Curtright AE, Arnold CB, Pique A, Swider-Lyons KE. Li-ion microbatteries generated by a laser direct-write method. *J Power Sources* 2004;126:193–202.
- [112] Pique A, Auyeung RYC, Kim H, Charipar NA, Mathews SA. Laser 3D micro-manufacturing. *J Phys D Appl Phys* 2016;49.
- [113] Atre AC, Arnold CB. LiCoO₂ texturing by laser induced forward transfer for printed microbatteries. *Proc SPIE* 2011;7921:0O1–8.
- [114] Atre AC, Arnold CB. LiCoO₂ texturing by laser induced forward transfer for printed microbatteries. *Proc SPIE* 2011;7921:0O1–8.
- [115] Rosenberg S, Hintennach A. Laser-printed lithium-sulphur micro-electrodes for Li/S batteries. *Russ J Electrochem* 2014;50:327–35.
- [116] Pröll J, Kim H, Mangang M, Seifert HJ, Piqué A, Pflęging W. Fs-laser microstructuring of laser-printed LiMn₂O₄ electrodes for manufacturing of 3D microbatteries. *Proc SPIE* 2014;8968:051–6.
- [117] Mangang M, Pröll J, Tarde C, Seifert HJ, Pflęging W. Ultrafast laser microstructuring of LiFePO₄ cathode material. *Proc SPIE* 2014;8968:0M1–9.
- [118] Pflęging W, Kohler R, Pröll J. Laser generated microstructures in tape cast electrodes for rapid electrolyte wetting – new technical approach for cost efficient battery manufacturing. *Proc SPIE* 2014;8968:0B1–8.
- [119] Choi J, Morikawa E, Ducharme S, Dowben PA. Comparison of crystalline thin poly(vinylidene (70%)-trifluoroethylene (30%)) copolymer films with short chain poly(vinylidene fluoride) films. *Mater Lett* 2005;59:3599–603.
- [120] Slocombe A, Li L. Laser ablation machining of metal/polymer composite materials. *Appl Surface Sci* 2000;154:617–21.
- [121] Cheng L, Crumlin EJ, Chen W, et al. The origin of high electrolyte-electrode interfacial resistances in lithium cells containing garnet type solid electrolytes. *Phys Chem Chem Phys* 2014;16:18294–300.
- [122] Hou HM, Cheng L, Richardson T, et al. Three-dimensional elemental imaging of Li-ion solid-state electrolytes using fs-laser induced breakdown spectroscopy (LIBS). *J Anal Atom Spectrom* 2015;30:2295–302.
- [123] Pflęging W, Smyrek P, Hund J, Bergfeldt T, Pröll J. Surface micro-structuring of intercalation cathode materials for lithium-ion batteries: a study of laser-assisted cone formation. *Proc SPIE* 2015;9351:1E1–12.
- [124] Smyrek P, Zheng Y, Rakebrandt JH, Seifert HJ, Pflęging W. Investigation of micro-structured Li(Ni_{1/3}Mn_{1/3}Co_{1/3})O₂ cathodes by laser-induced breakdown spectroscopy. *Proc SPIE* 2017;10092:0S1–7.
- [125] Zorba V, Syzdek J, Mao X, Russo RE, Kostecki R. Ultrafast laser induced breakdown spectroscopy of electrode/electrolyte interfaces. *Appl Phys Lett* 2012;100:234101.
- [126] Smyrek P, Zheng Y, Seifert HJ, Pflęging W. Post-mortem characterization of fs laser-generated micro-pillars in Li(Ni_{1/3}Mn_{1/3}Co_{1/3})O₂ electrodes by laser-induced breakdown spectroscopy. *Proc SPIE* 2016;9736:1C1–6.